UNIVERSITY OF CALIFORNIA,
IRVINE

Novel Computation for Fetal Electrocardiogram Extraction

DISSERTATION

submitted in partial satisfaction of the requirements
for the degree of

DOCTOR OF PHILOSOPHY

in Electrical Engineering

by

Sadaf Sarafan

Dissertation Committee:
Professor Hung Cao, Chair
Professor Tadesse Ghirmai
Professor Zhou Li

2022

DEDICATION

This thesis is dedicated to my parents for their endless love, support and encouragement. This work is also dedicated to my advisor for his guidance and support during my challenging research life.

TABLE OF CONTENTS

Page

LIST OF FIGURES vi

LIST OF TABLES ix

ACKNOWLEDGMENTS x

VITA xi

ABSTRACT OF THE DISSERTATION xiii

1 Motivation 1
- 1.1 Contributions and impact . . . 3
- 1.2 Dissertation outline . . . 3

2 Fetal ECG background 6
- 2.1 Introduction . . . 6
- 2.2 Fetal Electrocardiogram & Characteristics of the fECG . . . 6
- 2.3 Fetal monitoring . . . 9
  - 2.3.1 Fetal data acquisition . . . 9
- 2.4 Review of fetal ECG monitoring devices . . . 11
- 2.5 Summary . . . 13

3 Review of Non-Invasive Fetal ECG Analysis 15
- 3.1 Introduction . . . 15
- 3.2 Kalman Filter . . . 16
- 3.3 Blind Source Separation (BSS) . . . 20
  - 3.3.1 Independent Component Analysis (ICA) . . . 20
- 3.4 Template Subtraction . . . 22
- 3.5 TS and ICA combination . . . 24

4 Database and Evaluation Criteria 27
- 4.1 Introduction . . . 27
- 4.2 Data . . . 27
  - 4.2.1 Online Data: PhysioNet 2013 Challenge databank . . . 27
  - 4.2.2 Own Clinical Data . . . 28
  - 4.2.3 Online Data: MIT-BIH Noise Stress Test Database . . . 29

4.2.4 Modified Online Data . . . 29
4.3 QRS detection . . . 32
4.3.1 Pre-Processing . . . 32
4.4 Comparison Criteria . . . 33
4.4.1 QRS detection accuracy . . . 33
4.4.2 Noise reduction performance . . . 34
4.5 Summary . . . 35

5 A Fetal ECG Monitoring System Based on the Android Smartphone 36
5.1 Introduction . . . 36
5.2 Methods and Implementation . . . 38
5.2.1 The fetal patch . . . 38
5.2.2 Fetal ECG Extraction Algorithm . . . 39
5.2.3 Android Smartphone App Software . . . 40
5.3 Results . . . 41
5.3.1 Algorithm Validation . . . 41
5.3.2 Device Validation . . . 42
5.3.3 Entire System Validation . . . 43
5.4 Discussion . . . 45

6 Novel Approaches for Non-Invasive Fetal ECG Extraction 47
6.1 Introduction . . . 47
6.2 Theory and Method . . . 48
6.2.1 Review of Extended Kalman Filter . . . 48
6.2.2 Ensemble Kalman Filter (EnKF) . . . 49
6.3 EnKF based fECG Extraction Algorithm . . . 53
6.3.1 State-Space Model of a Synthetic ECG . . . 53
6.3.2 Fetal QRS Detection with EnKF . . . 56
6.3.3 Preprocessing . . . 57
6.4 Results . . . 57
6.5 Discussion . . . 62

7 ECG Denoising Using the EnKF 65
7.1 Introduction . . . 65
7.2 Review of ECG denoising methods . . . 65
7.3 Methods . . . 66
7.4 Results . . . 67
7.5 Discussion . . . 70

8 Comparison of Methods to Extract Fetal Electrocardiogram 74
8.1 Introduction . . . 74
8.2 Methods . . . 75
8.3 Results . . . 76
8.4 Discussion . . . 82

9 Conclusion and Prospective **85**
9.1 Summary of contributions 85
9.2 Conclusion 86
9.2.1 fECG extraction Algorithms 86
9.2.2 Home-based Fetal Electrocardiogram (ECG) Monitoring System . . . 86
9.2.3 A Novel Algorithm for fECG Extraction 87
9.2.4 Novel Algorithm for ECG denoising 88
9.3 Future works 89

Bibliography **90**

LIST OF FIGURES

Page

2.1 The activation cycle of the fetal heart; adopted with permission from [1]. . . 7
2.2 ECG waveform with characteristic waves. 8
2.3 Typical fetal acoustic heart sound signal [2]. 10
2.4 Example of a abdominal ECG signal. The fQRS annotation is shown in orange asterisk (*). 12
2.5 Examples of FDA-certified commercially available based on Doppler technology (HeraBEAT) [3]. 13
2.6 Commercially available NI-fECG-based devices. (a) Monica Novii Wireless Patch System [4, 5]; (b) MERIDIAN M110 Fetal Monitoring System [4, 5]; (c) Philips Avalon Beltless [6]; (d) Nemo Fetal Monitoring System [4, 5]. . . 14

3.1 Kalman Filter Algorithm. 17
3.2 EKF linearizing a non-linear function around the mean of a Gaussian distribution. 19
3.3 Extended Kalman Filter Algorithm. 20
3.4 FastICA algorithm. 22
3.5 RobustICA algorithm. 23
3.6 Template subtraction (TS)'s illustration for aECG. 24
3.7 fQRS detection process: (1) Preprocessing step with notch filter, high pass filter and low pass filter utilized; (2) The Pan-Tompkins algorithms applied for mQRS detection used to create a template mECG and for channel selection in independent component analysis (ICA) method; (3) Source separation includes different approaches (TS, ICA and its hybrid). For ICA and the hybrid method, the extracted signals contain 4 signals (i.e., fECG, mECG and two noise signals; (4) Using mQRS detection from (2) as a criterion for fECG selection; (5) The Pan-Tompkins algorithm applied for fQRS detection. . . . 26

4.1 The fetal monitoring patch is a self-administered device consisting of non-contact electrodes, electronics, and BLE worn by the pregnant woman. The wireless fetal heart monitoring prototype in use at UCI Medical Center. . . . 29
4.2 Implementation of motion noise generation procedure. 30
4.3 Illustration of applying noise to record a01 motion, (a) Normalized a01 record, (b) Generated motion noise, (c) a01 with added motion noise artifact. 31

5.1 Fetal ECG monitoring system overview. 37

5.2 The NCE ECG obtained by our system and an ECG denoising example. . . 37
5.3 Fetal ECG monitoring patch and system. 38
5.4 Fetal ECG monitoring patch and system. 40
5.5 Android application operation flow chart. 41
5.6 Results of fetal ECG Extraction by using the Mobile app and MATLAB. (a) A signal from PhysioNet 2013 Challenge databank; and (b) the fECG signal on Mobile app and MATLAB. 42
5.7 The fetal patch setup and experiment. 43
5.8 ECG signals recorded from the patch: (a) sitting position, (b) standing position, (c) walking position. 44
5.9 Real-time monitoring/altering android smartphone app software. 44
5.10 Results of fetal ECG extraction by using the Android application. (a) recorded data from maternal abdominal; (b) filtered data; and (c) Fetal ECG extracted and fetal QRS detected. 45

6.1 An overview of EnKF. EnKF maintains an ensemble of sample points for the state vector x_n. It propagates and updates the ensemble to track the distribution of x_n. The state estimation is conducted by calculating the sample mean (red five-pointed-star) and covariance (red ellipse) of the ensemble. . . 54
6.2 Fetal QRS (fQRS) detection process: (1) Preprocessing step ; (2) Ensembel Kalman filter (EnKF) applied for maternal ECG (mECG) extraction; (3) mECG subtracted from filtered aECG signal and EKF used for fetal ECG (fECG) extraction; (4) EnKF applied for fECG extraction. 56
6.3 A phase-wrapped ECG signal of records "a01". (a) Abdominal ECG (raw data); (b) mECG extracted using EKF; and (c) mECG extracted using our EnKF. 58
6.4 fECG extraction using the EKF and EnKF with the PhysioNet data. The fQRS annotation is shown in orange asterisk (*). The red arrows show the places that fetal QRS was wrongly detected. The blue arrows show the missing fetal QRS. (a) Abdominal ECG (raw data) of record "a03"; (b) fECG extracted using EKF of record "a03"; (c) fECG extracted using EnKF of record "a03"; (d) Abdominal ECG (raw data) of record "a01" with reversed fetal QRS complexes; (e) fECG extracted using EKF of record "a01"; (f) fECG extracted using EnKF of record "a01". (g) Abdominal ECG (raw data) of record "a01" with reversed fetal QRS complexes; (h) fECG extracted using EKF of record "a01"; (i) fECG extracted using EnKF of record "a01". . . . 60
6.5 fECG extraction using the EKF and EnKF with the motion artifacts added PhysioNet data. The fQRS annotation is shown in orange asterisk (*). The red arrows show the places that fetal QRS was wrongly detected. The blue arrows show the missing fetal QRS. (a) Abdominal ECG (raw data); (b) fECG extracted using EKF; and (c) fECG extracted using EnKF. 61

6.6 fECG extraction using the EKF and EnKF with our own clinical data. The fQRS annotation is shown in orange asterisk (*). The red arrows show the places that fetal QRS was wrongly detected. The blue arrows show the missing fetal QRS. (a) Abdominal ECG (raw data), (b) fECG extracted from EKF and (c) fECG extracted from EnKF". (d) Abdominal ECG after Wavelet preprocessing; (e) fECG extracted using EKF of preprocessed data; and (f) fECG extracted using EnKF of preprocessed data. The inset shows additional peaks, likely P and T waves; they were conserved after EnKF extraction. . . 62

7.1 The EnKF algorithm flow chart. 67
7.2 phase-wrapped ECG filtering results for an input signal of 12 dB. (a) EnKF. (b)EKF. (c) SG. (d) Wavelete. (e) EEMD Filter. (f) LMS Adaptive Filter. (g) RLS Adaptive Filter. (h) Total Variation Denoising. 68
7.3 Enhanced ECG signals in time domain obtained by using different denoising methods. (a) EnKF. (b)EKF. (c) SG. (d) Wavelete. (e) EEMD Filter. (f) LMS Adaptive Filter. (g) RLS Adaptive Filter. (h) Total Variation Denoising. 70
7.4 (a) Comparison of the mean RMSE obtained by using different denoising methods at different input SNR levels. (b) Comparison of the mean Correlation versus different input SNR levels. (c) Comparison of the PRD for different denoising methods at different input SNR levels. (d) Comparison of the mean SNR improvements for different denoising methods versus different input SNR levels. 71

8.1 fQRS detection illustrated by TS method: (a) the aECG signal is filtered baseline wander and power line and applied Pan-Tompkins for mQRS detection; (b) a template of mECG is constructed from filtered aECG and the R peaks of mECG; (c): the residual signal is derived by the subtraction between filtered aECG and template mECG and Pan-Tompkins is applied for fQRS detection. The fQRS annotation is also included (plus sign in green). 76
8.2 F1 comparison with different Gaussian noise levels. 80
8.3 The time execution comparison. 82

9.1 The fetal ECG monitoring system in operation. (a) Wearable fECG monitoring system attached to the maternal abdomen; (b) Wearable fECG monitoring system attached to the maternal abdomen; and (c) Android phone client main interface. 87

LIST OF TABLES

Page

5.1 Average F1 score (%) with mobile app and MATLAB code for all records . . 42

6.1 Performance of the EKF and EnKF algorithms. 61

7.1 Performance of denoising of algorithms for the motion noise cancellation. . . 72

8.1 Average F1 score(%) with different methods. 78
8.2 Number of records out of 68 datasets with F1 scores less than 50%. 79
8.3 Required memory for different methods. 81

ACKNOWLEDGMENTS

This thesis would not have been possible without the support of numerous people. I would like to express my sincere gratitude to my adviser Prof. Hung Cao for his unwavering support and believing in me. I want to thank Prof. Cao for giving me the opportunity to do my PhD in his research group. His immense knowledge and plentiful experience have encouraged me in all the time of my academic research and daily life. I would like to thank all the members in the Hero Lab. It is their kind help and support that have made my study and life a wonderful time. Also thanks to my committee members, Prof. Tadesse Ghirmai, Prof. Zhou Li, Prof. Amir Rahmani and Prof. Jim Brody, who offered guidance and support.

I am also immensely grateful for Dr. Tadesse Ghirmai. I am so lucky to have benefited not only from his incredible scientific insight, but also from his immense kindness and empathy. I am also extremely thankful for his consistent support and help.

My sincere thanks also goes to Dr. Afshan Hameed at University of California, Irvine Medical Center for providing invaluable comments and suggestions and who gave access to the University of California, Irvine Medical Center to he entire system on pregnant women. Without they precious support it would not be possible to conduct this thesis.

I would like to thank the funding resources: the National Science Foundation (NSF) CAREER Award 1917105 (H.C.), the National Institutes of Health (NIH) R44 OD024874 (M.P.H.L. and H.C.), and the Proof of Product (POP) Grant from the UC Irvine's Beall Applied Innovation (H.C.).

My family: my father Rashid, my mother Beheshteh, my brother Arian and my sister Yasaman for their continuous support and encouragement over the years and in particular to my parents for your immense patience during the tough times, and for always encouraging me to set lofty goals and achieve them. You constantly inspire me to become a better person and to enjoy life to its fullest. Thank you to my friends, Dr. Diba Golchin and Dr. Kaveh Shahverdi, for all of the kind words and assistance they have provided.

VITA

Sadaf Sarafan

EDUCATION

Doctor of Philosophy in Electrical Engineering **2022**
University of California, Irvine *Irvine, CA*

Master of Science in Electrical Engineering **2017**
Shahid Beheshti University *Tehran, Iran*

Bachelor of Science in Electrical Engineering **2014**
Shahid Beheshti University *Tehran, Iran*

RESEARCH EXPERIENCE

Graduate Research Assistant **2018–2022**
University of California, Irvine *Irvine, California*

Graduate Research Assistant **2014–2018**
Shahid Beheshti University *Tehran, Iran*

TEACHING EXPERIENCE

Teaching Assistant (Electrical Engineering Analysis) **2022–2022**
University of California, Irvine *Irvine, CA*

Teaching Assistant (Network Analysis I) **2021–2021**
University of California, Irvine *Irvine, CA*

Teaching Assistant (Electrical Engineering Analysis) **2021–2021**
University of California, Irvine *Irvine, CA*

Teaching Assistant (Network Analysis I) **2020–2020**
University of California, Irvine *Irvine, CA*

Teaching Assistant (Introduction to Digital Systems) **2019–2019**
University of California, Irvine *Irvine, CA*

Teaching Assistant (Electrical Engineering Analysis) **2019–2019**
University of California, Irvine *Irvine, CA*

Teaching Assistant (Introduction to Digital Logic Laboratory) **2019–2019**
University of California, Irvine *Irvine, CA*

Teaching Assistant (Channel Coding) **2016–2016**
Shahid Beheshti University *Tehran,Iran*

REFEREED JOURNAL PUBLICATIONS

Investigation of Various Methods to Extract Fetal Electrocardiogram from the Mother's Abdominal Signal in Practical Scenarios **2020**
Technologies

Simultaneous Cardiac and Neurological Monitoring to Assess Chemical Exposures and Drug Toxicity in Xenopus Laevis **2022**
Biosensors and Bioelectronics

Fetal Electrocardiogram Extraction from the Mother's Abdominal Signal Using the Ensemble Kalman Filter **2022**
Sensors

A Novel QRS Detection Algorithm Based on the Adaptive Improved Permutation Entropy **2022**
bioRxiv

Fetal ECG extraction from single-channel abdominal ECG using Adaptive Improved Permutation Entropy **2022**
bioRxiv

REFEREED CONFERENCE PUBLICATIONS

Development of a Home-based Fetal Electrocardiogram (ECG) Monitoring System **2021**
43rd Annual International Conference of the IEEE Engineering in Medicine & Biology Society

A Novel ECG Denoising Scheme Using the Ensemble Kalman Filter **2022**
44rd Annual International Conference of the IEEE Engineering in Medicine & Biology Society

ABSTRACT OF THE DISSERTATION

Novel Computation for Fetal Electrocardiogram Extraction

By

Sadaf Sarafan

Doctor of Philosophy in Electrical Engineering

University of California, Irvine, 2022

Professor Hung Cao, Chair

Fetal electrocardiogram (fECG) assessment is essential throughout pregnancy to monitor the well-being and development of the fetus, and to possibly diagnose potential congenital heart defects. Due to the high noise incorporated in the abdominal ECG (aECG) signals, the extraction of fECG has been challenging. And it is even a lot more difficult for fECG extraction if only one channel of aECG is provided, i.e., in a compact patch device. Our team has been developing a novel wearable fECG monitoring system consisting of an abdominal patch that communicates with a smart device. The system has two main components: the fetal patch and the monitoring app. The fetal patch has electronics and recording electrodes fabricated on a hybrid flexible-rigid platform while the mobile app is developed for a wide range of applications. The patch collects the aECG signals and send them to the app via secure Bluetooth Low Energy (BLE) communication. The app software connects to a cloud server where processing and extraction algorithms are executed for real-time fECG extraction and fetal heart rate (fHR) calculation from the collected raw data.

This thesis work focuses on algorithms for fECG extraction from the aECG signals of a pregnant mother including a novel scheme based on the Ensemble Kalman filter (EnKF) for extraction from a single-channel aECG signal. The EnKF algorithm is developed by considering a Bayesian filtering framework and formulating the fECG extraction problem as a dynamic system whose state and measurement equations are represented in a state-space

form. Our work has the potential to transform the currently used fetal monitoring system to an effective distanced and tele-perinatal care.

Chapter 1

Motivation

According to the Centers for Disease Control (CDC), cardiovascular diseases have become the first leading cause of death of all deaths occurring in the United States in 2017 [7]. According to the European Health Network European Cardiovascular Disease Statistics 2017 edition, each year cardiovascular disease causes 3.9 million deaths in Europe and over 1.8 million deaths in the European Union (EU) [8]. Assessment of an electrocardiogram (ECG) will provide vital information about a heart condition, and the existence of abnormalities or distress. However, ECG recordings, especially by portable devices are commonly contaminated by outside interferences referred to as 'noise artifacts'. These noise artifacts are a conglomerate of common noises such as motion noise, baseline wander, and powerline interference, just to name a few. Despite the recent advances in signal processing, there is still no efficient method for denoising biopotentials acquired by wearables, such as ECG. The ECG recordings are commonly distorted and contaminated by noise artifacts. Therefore, the extraction of high-resolution ECG signals from noisy measurements is required.

A national study reported by the CDC showed that the U.S. fetal mortality rate remained unchanged from 2006 through 2013 from the rate of 6.05 to 5.96 per 1,000 births [9]. The

infant mortality rate in the United States shows no improvement in the care system with 6.20 per 1,000 live births in 2004 and 6.23 in 2003 [10]. Thus, fetal heart rate monitoring (fHR) is an essential component of perinatal care by recognizing elements that might imperil the life of the fetus and mother. Fetal electrocardiogram (fECG) provides vital information about fetal well-being, fetal development, and maturity, or non-reassuring fetal status during pregnancy and labor [11][2]. The fECG extraction from maternal abdominal recordings is not an easy task. The low signal-to-noise-ratio (SNR) of fECG and the appearance of other signals, namely maternal ECG (mECG), baseline wander, and noise, bring challenges. A number of reports have been presented on the development of new signal processing techniques to tackle such issues.

The current global COVID-19 pandemic has led to critical demand for per-son-centered healthcare instead of hospital-centered healthcare system. Expectant moms usually come to the obstetric clinics many times during pregnancy for checkups. According to the CDC, a study on 461,825 women with COVID-19 showed that pregnant women with COVID-19 are more likely admitted to an intensive care unit, receiving invasive ventilation, extracorporeal membrane oxygenation, or die compared with non-pregnant women [12]. This would stop pregnant women from having physio-logical measurements, ultrasound examinations, or non-stress tests, which are critical for both the mom and the unborn baby. This calls for an urgent need for novel home-based tools and systems for reliable prenatal monitoring.

All methods that performed greatly for fECG extraction required multiple-channel abdominal ECG (aECG) signal, which makes them unsuitable for continuous non-invasive fECG monitoring [13]. Also, the high noise level in daily life renders long-entrenched challenges to extract fECG from the combined fetal/maternal ECG signal recorded in the abdominal area of the mother [13]. Therefore, a robust scheme to provide home-based fHR monitoring from a compact device acquiring a single-channel aECG signal with the presence of high noise is required.

1.1 Contributions and impact

This doctoral work focuses on a novel signal processing algorithm to tackle the problem of low SNR in NI-fECG recordings and extract the fECG from the aECG. This algorithm is more robust and close to optimal performance as precise fECG is preferred for fetal monitoring. The contributions of this thesis are summarised below:

- Simulated data by adding motion noise to the data mimicking to the situation with wearable devices in daily life, to obtain a thorough view of the effectiveness and robustness in practical scenarios. See Chapter 4 and the journal paper [13]
- Development of a Home-based fECG Monitoring System. See Chapter 5 and the conference paper [14].
- Novel algorithm based on the Ensemble Kalman filter (EnKF) to extract fECG from a single-channel aECG signal. See Chapter 6 and the corresponding journal paper [15]
- Development of a novel algorithm based on the Ensemble Kalman Filter to remove noise in ECG signals. See Chapter 7 and the conference paper [16].
- Review of existing NI-fECG extraction approaches. A thorough and comprehensive review of NI-fECG extraction approaches was conducted. See Chapter 8 and the corresponding journal paper [13].

1.2 Dissertation outline

The objective of this work is to tackle the problem of the current fetal ECG extraction algorithms. The thesis was divided into three logical parts, which are addressed in this dissertation, as follows. **Chapter 2** introduces the methods that are currently used in clinical

practice and research for fetal monitoring, development of fECG monitor, and factors that may influence the fetal cardiac activity are described.

In **Chapter 3**, the various extraction algorithms are provided, including concepts of the Extended Kalman filter (EKF), relevant for the novel proposed algorithm. This chapter reviews the 'state of the art' in the field of signal processing for NI-fECG extraction.

Chapter 4 presents databases, tools, and materials that are used throughout this work for validating the proposed. The aECG recordings acquired in real-life settings would possess a variety of interferences, including motion artifacts. The online databank, however, was obtained in the clinical setting, where motion noise was mostly non-existent since the subjects were in a resting position. The realistic motion noise generation process is described in this chapter, to mimic real-life scenarios.

A home-based fetal ECG monitoring system has been developed, in **Chapter 5**. The system was validated and compared with both simulated data and online data. We applied for Institutional Review Board (IRB) protocols to conduct validations with pregnant women in our participating clinics at the University of California Irvine, CA (IRB2020-6342).

In **Chapter 6** a nonlinear Bayesian filtering framework is proposed for fetal ECG extraction. The EnKF was created from the combination of Kalman filter theory and Monte Carlo estimation methods [17]. This chapter provides the theoretical background and overview of the EnKF method. Finally, the EnKF is evaluated on our own clinical data, obtained from a pilot study with 10 subjects each of 20 min recording, and data from the PhysioNet 2013 Challenge bank with labeled QRS complex annotations.

Chapter 7 presents a nonlinear Bayesian filtering framework for the filtering of single-channel noisy electrocardiogram (ECG) recordings. Quantitative evaluation of the proposed algorithm on the MIT-BIH signals and the modified MIT-BIH database with added motion artifacts demonstrate the reliability and effectiveness of the EnKF. The EnKF is able to re-

move different types of noises with minimum signal distortion. Concerning the high accuracy of this method, it can be widely used in home ECG monitoring devices.

In **Chapter 8**, various extraction algorithms are intensively explored, including template subtraction (TS), independent component analysis (ICA), and extended Kalman filter (EKF) using the data from the PhysioNet 2013 Challenge. Furthermore, the modified data with Gaussian and motion noise added, mimicking a practical scenario, were utilized to examine the performance of algorithms. Finally, different algorithms are combined together, yielding promising results. It should be noted that these combined approaches required higher computational complexity, including execution time and allocated memory compared with other methods. Owing to comprehensive examination through various evaluation metrics in different extraction algorithms, this chapter provides insights into the implementation and operation of state-of-the-art fetal and maternal monitoring systems in the era of mobile health.

Chapter 9 summarises the finding of this research, and the strengths as well as weaknesses in comparison with other algorithms. Future works are also presented.

Chapter 2

Fetal ECG background

2.1 Introduction

This chapter provides the physiological concepts, technical background of fetal electrocardiogram (fECG), and fetal monitoring methods that are currently used. special focus is given to the development of the fECG modality and to the information that can be extracted from this physiological signal. We will review a selection of the available literature with special focus on the most significant ones, which have been specifically developed for the problem of interest.

2.2 Fetal Electrocardiogram & Characteristics of the fECG

The Dutch physiologist Willem Einthoven developed the first electrocardiogram in 1903 [18]. In the late 1960s, computerized electrocardiography was used in many larger hospitals [19].

An electrocardiogram or ECG is a simple display of the electrical activity of the heart muscle and its changes over time, which are often printed on a piece of paper for easier analysis. Like other muscles, the heart muscle contracts in response to the electrical depolarization of muscle cells. In fact, ECG is the sum of these electrical activities that are amplified and recorded in a few seconds. An ECG signal is recorded by placing electrodes in different parts of the surface of the body. Figure 2.1 illustrates the electrical pathway through the fetal heart and how this propagation translates into the characteristic waves that are observed on the ECG signal. It should be noted that some functional differences between the fetus and adult hearts are exist [20]. Despite the functional differences between the fetus and adult hearts, the electrical activity is partly similar [20]. There are 5 main components to an ECG: P, Q,

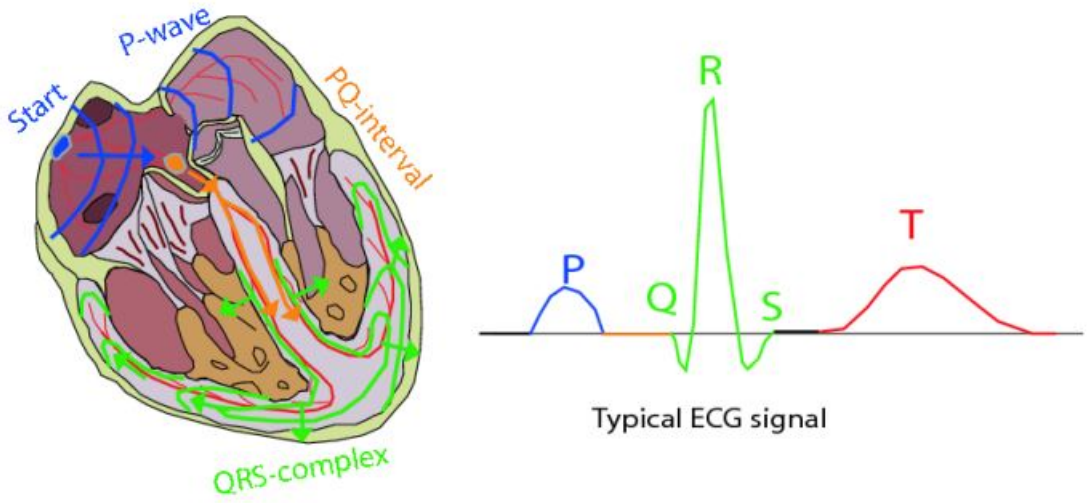

Figure 2.1: The activation cycle of the fetal heart; adopted with permission from [1].

R, S, T corresponding to different phases of the heart activities. The P wave represents the normal atrium (upper heart chambers) depolarization; the QRS complex corresponds to the depolarization of the right and left ventricles (lower heart chambers); the T wave represents the re-polarization of the ventricles. To interpret ECG, the heart rate, shape, and size of each wave and the timing should be considered. The ECG waveform with characteristic waves is depicted in Figure 2.2. The fECG is similar to the adult ECG, and contains the

five characteristic waves (P, Q, R, S, and T). Although the structure and morphology of the fECG contain more invaluable information for prognosis and therapeutic potentials than the heart rate, many fetal ECG extraction methods have only extracted the R-R intervals using the detection of R-peaks or the overall result of the ECG waveform. This is due to the relatively low signal-to-noise ratio (SNR) of the fECG compared to the mECG, which in itself makes the structure and morphology of fECG a challenging issue.

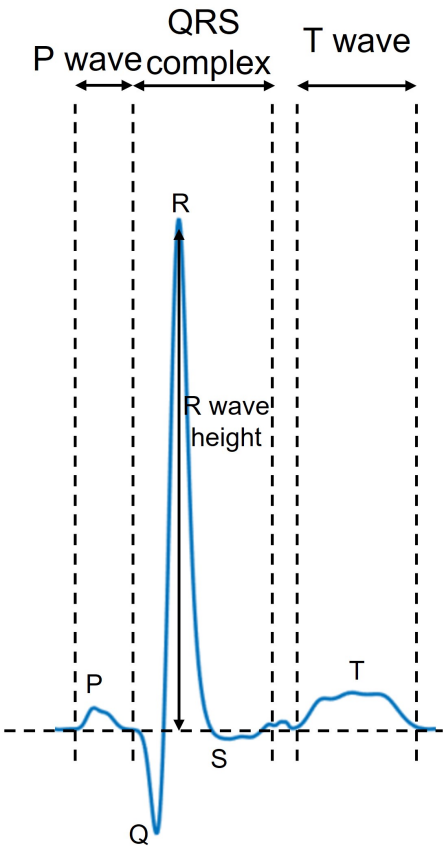

Figure 2.2: ECG waveform with characteristic waves.

2.3 Fetal monitoring

The number of reported pregnancy-related deaths in the U.S. steadily increased from 18.8 maternal deaths per 100,000 live births in 2000 to 23.8 deaths per 100,000 live births in 2014 [21]. One of the most frequent birth abnormalities and the major cause of mortality from birth disorders is congenital heart disease (CHD) [22, 23]. Genetics, inherited disorders, or environmental factors such as infection or drug abuse may be associated with CHD and cardiac malformations [24]. Early detection is of critical importance and can increase survival rates. Thus, fetal monitoring is essential throughout pregnancy for the recognition of elements that might imperil the life of the fetus and mother. Monitoring the fetal heart condition can help to diagnose problems such as preterm delivery, hypoxia, intrauterine growth retardation, etc., which may not only pose a risk to the fetus but also to maternal health [11].

2.3.1 Fetal data acquisition

Cardiotocography (CTG) is widely used to monitor fetal health. A key fetal monitoring parameter, which is fetal heart rate (fHR) via CTG, despite being used in 85% of all labors in the U.S., and with comparable frequency during the antepartum period for monitoring, has not unequivocally shown that it can reduce perinatal mortality. The traditional CTG-based non-stress test (NST) and contract stress test (CST) for fetal health assessment are all done in the clinic or hospital under the supervision of a healthcare professional. The current CTG uses the Doppler ultrasound method to measure fHR. It is performed by transmitting an ultrasound beam through the maternal abdomen and measuring the frequency of the reflected signal [25]. Echocardiography, also known as sonography, is based on standard ultrasound techniques. Such measurement could be challenging at times due to the need for precise alignment with the fetal heart to detect the fHR, which could be difficult when

there are excessive maternal or fetal movements, or in the case of maternal obesity [26]. The drawbacks of traditional CTG systems are: 1) high cost; 2) useless outside of the hospital setting and 3) bulky and complicated equipment.

To overcome the fHR measurement difficulties for CTG using the Doppler method, especially needed during a situation of possible fetal distress when fHR assessment is absolutely critical, obstetricians have resorted to measuring fHR by the more reliable method of using fECG, which currently can only be obtained through a scalp electrode directly attached to the fetal scalp [27]. However, this is an invasive procedure and can only be done after the rupture of the amniotic membrane, potentially causing some risks such as infection.

The other CTG measurement is a fully non-invasive acoustic recording called phonocardiography (PCG) [28]. PCG is a graphic registration of the heart sounds and murmurs produced by the contracting heart [29]. Although this measurement is inexpensive and non-invasive, but the acoustic signal recorded on the maternal abdominal surface is contaminated by undesired signals such as acoustic damping through the fruit water and tissues, the noise produced by the fetal movements, sounds of maternal heart activity, and surrounding environment noise [28, 30]. The obesity of the mother may prevent PCG recording. Figure 2.3 illustrates the typical fetal acoustic heart sound signal (fPCG). It can be seen that each heartbeat can be separated into two parts: an S1 (systolic) beat, followed by a softer S2 (diastolic) beat.

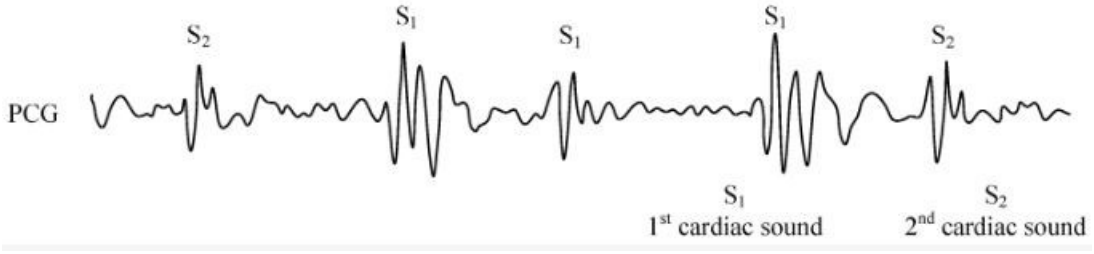

Figure 2.3: Typical fetal acoustic heart sound signal [2].

Alternative fetal monitoring methods over the last few decades are the bioelectric activity of the fetal heart [4, 31]. Most heart defects and CHD are captured on the cardiac electrical signals, which are recorded by electrocardiography and are believed to contain more information than conventional sonographic methods [32]. The fECG provides useful information on both fetal heart rate and fetal heart condition. The fECG can be recorded in two ways; through an electrode attached to the fetal scalp while the cervix is dilated, also known as direct fetal electrocardiography (invasive fECG), or non-invasively through electrodes attached to the mother's abdomen. Figure 2.4 shows an example of an abdominal electrocardiogram (aECG) recorded simultaneously. Due to obtaining the NI-fECG from the surface of the abdomen, the aECG is always accompanied by other bioelectric potentials like maternal heart activity, fetal heart activity, maternal muscle activity, fetal movement activity, and noise [33]. The quality of this signal depends on the position of the fetus, the location of the electrode, the developmental stage of the fetal heart, and the environment noise [34, 35, 36, 37]. The mECG and fECG signals overlap in both the time and frequency domain. Therefore, continuous and noninvasive fECG monitoring has remained a challenging problem in the research community. While strides have been made lately in sensing technology and signal processing to enhance the signal-to-noise ratio (SNR) of aECG signals, the monitoring, and analysis of fECG are still immature [38]. In chapter 3, an overview of the NI-fECG signal processing is provided.

2.4 Review of fetal ECG monitoring devices

In recent years, home-based devices for fetal monitoring have been introduced. Those include hand-held ultrasound fHR monitor devices. The HeraBEAT device (HeraMED, Netanya, Israel) employs ultra-wide beam Doppler technology. However, these devices have technical limitations, such as signal loss with high body-mass-index (BMI) mothers, and high risk to

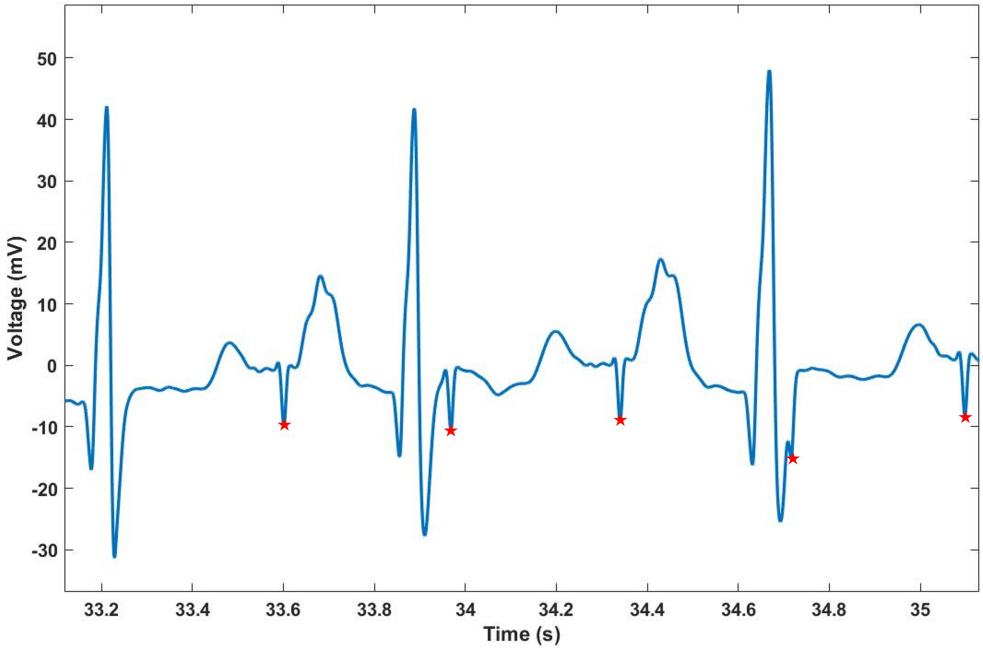

Figure 2.4: Example of a abdominal ECG signal. The fQRS annotation is shown in orange asterisk (*).

the safety of pregnant ladies and fetuses [39, 40]. Further, they can assess the heart rate and provide no indication of other important functional conditions of the heart.

Besides the in-hospital/clinic CTG clinical application, such fHR/fECG assessment using non-invasive sensors on the abdomen of the pregnant mother can be used for the home-based fetal heart monitoring applications, opening up a new dimension for antepartum and intrapartum wellbeing assessment and monitoring. For fECG-based systems, there are four major providers. MindChild Medical has developed the MERIDIAN M110 system. It overcomes the limitations of traditional CTG; however, the system is wire-connected, bulky, expensive, and non-mobile. The GE Monica Novii wireless patch system (GE, USA, formerly the Monica Healthcare Novii) uses less bulky fECG sensors and it is wireless. However, the mobile range is limited to the labor and delivery areas in the hospital. They are all very costly, and not affordable for consuming customers. The Philips Avalon Beltless (Philips, the Netherlands) has cableless connections. However, this device must be used in a hospital

Figure 2.5: Examples of FDA-certified commercially available based on Doppler technology (HeraBEAT) [3].

and can not be used at home [6]. The Nemo Fetal Monitoring System (Nemo Healthcare, the Netherlands) is a wireless fetal monitoring device. It provides the uterine electromyography (EMG) signal [41]. Its performance is strongly dependent on location, timing, maternal activity levels, and maternal posture.

2.5 Summary

In this chapter, the physiology and electrophysiology of the fetal were reviewed. We also presented a number of NI-fECG extraction techniques that are used. The advantages and disadvantages of each group are described.

Different home HR monitoring devices are described. fHR can be done via 1) fECG extraction from aECG or 2) Doppler ultrasound like CTG systems. There are already existing ultrasound-based consumer products for fHR assessment in the home setting. Those require active scanning over the abdomen coupling with ultrasound gel to locate the fetal heart to obtain the fHR, which is highly technique dependent, easily make difficult by maternal or fetal movement and larger body size. Thus, it is especially challenging for non-medical persons to administer it. Home-based fECG systems were developed and introduced; however, they are bulky, costly, and intrusive, thus not widely used. Further, the lack of effective and

(a)

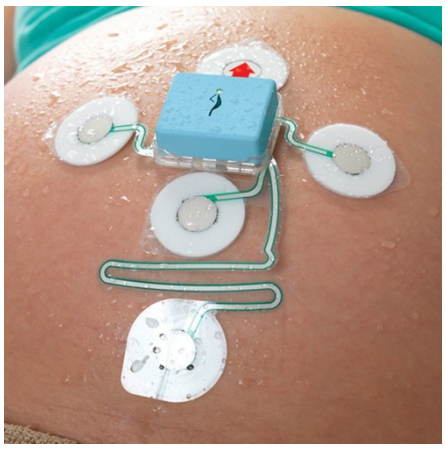

(b)

(c)

(d)

Figure 2.6: Commercially available NI-fECG-based devices. (a) Monica Novii Wireless Patch System [4, 5]; (b) MERIDIAN M110 Fetal Monitoring System [4, 5]; (c) Philips Avalon Beltless [6]; (d) Nemo Fetal Monitoring System [4, 5].

robust signal processing has limited those to only fetal heart rate monitoring.

Chapter 3

Review of Non-Invasive Fetal ECG Analysis

3.1 Introduction

There are several methods proposed for extracting fetal electrocardiogram (fECG) from abdominal electrocardiogram (aECG). These methods can be generally classified into three groups: blind source separation (BSS), template subtraction (TS), and filtering techniques. The BSS methods include methods such as parallel linear predictor (PLP) filter, principle component analysis (PCA), independent component analysis (ICA), and periodic component analysis (πCA) [37, 42, 43, 44]. The BSS methods consider that the abdominal signal is a combination of fECG, mECG, and noises [26]. Although these methods perform greatly for fECG extraction, they need multiple-channel aECG signals, which makes them unsuitable for continuous non-invasive fECG monitoring. In addition, after extraction, the order of the separated independent component could not be determined, thus it is challenging to identify the fECG component for further processing [45]. Therefore, the BSS methods usually require

the determination of other parameters (e.g., t-test, correlation coefficient, heart rate) to automatically identify the extracted components [46, 47, 48]. TS is another widely used approach. The method involves subtracting a synthetic mECG generated by estimating the QRS complex waveform (mQRS) of mECG from the abdomen signal [49, 50, 51, 52, 53, 54]. The main challenge of this method involves mQRS detection [55], which becomes more challenging if the fetal R waves overlap with the maternal R waves. This drawback degrades the effectiveness of the template subtraction method for fECG extraction. The popular filtering techniques include adaptive filtering [56, 57, 58, 59], Kalman filtering [60, 61, 62], and wavelet transform [63, 64]. These filtering techniques are mostly and effectively applied for denoising of single-channel ECG signals. Adaptive filtering-based algorithms have been proposed for fECG extraction [65]. Such methods, however, require additional reference signals for separating the different components of the aECG. Some popular algorithms used for fetal ECG extraction are described in detail in the following.

3.2 Kalman Filter

Bayesian filtering is a probabilistic technique that uses incoming measurements $\mathbf{y}$ and a mathematical process model to recurrently estimate the posterior distribution of a hidden state random variable $\mathbf{x}$ at each time k [16]. The conventional Kalman Filter (KF) assumes a linear model for the system dynamics and observation equations. In practice, however, most systems are nonlinear in nature. A dynamic model of the system is written:

$$\begin{cases} y_n = Hx_n + w_n \\ x_n = Ax_{n-1} + u_n \end{cases} \tag{3.1}$$

We assume that u_n and w_n correspond to the process and observation noise which have no bias: $E[w_n] = 0$, $E[u_n] = 0$, and have a covariance matrices $Q_n = E\{u_n {u_n}^T\}$ and

$R_n = E\{w_n {w_n}^T\}$ respectively.

$$\begin{aligned} \hat{x}_{n|n-1} &= A\hat{x}_{n-1} + Bu_{n-1} \\ P_{n|n-1} &= AP_{n-1}A^T + Q \end{aligned} \tag{3.2}$$

where $\hat{x}_{n|n-1}$ is the predicted value of the state vector, $P_{n|n-1}$ is the covariance of the error of the predicted state vector given by $P_{n|n-1} = E[(\hat{x}_n - \hat{x}_{n|n-1})(\hat{x}_n - \hat{x}_{n|n-1})^T]$, and $E[.]$ is the expectation operator. Once the measurement vector is received, the measurement update step is used to compute the estimate of the state vector, $\hat{x}_n$ and the covariance of the error of the state vector, P_n, by applying corrections to the corresponding predicted values based on the measurement obtained as follows:

$$\begin{aligned} K_n &= P_{n|n-1}H^T(HP_{n|n-1}H^T + R)^{-1} \\ \hat{x}_n &= \hat{x}_{n|n-1} + K_n(y_n - H\hat{x}_{n|n-1}) \\ P_n &= (I - K_nH)P_{n|n-1} \end{aligned} \tag{3.3}$$

where K_n is the Kalman gain, and I is a diagonal matrix. Figure 3.1 shows a complete basic operation of the KF.

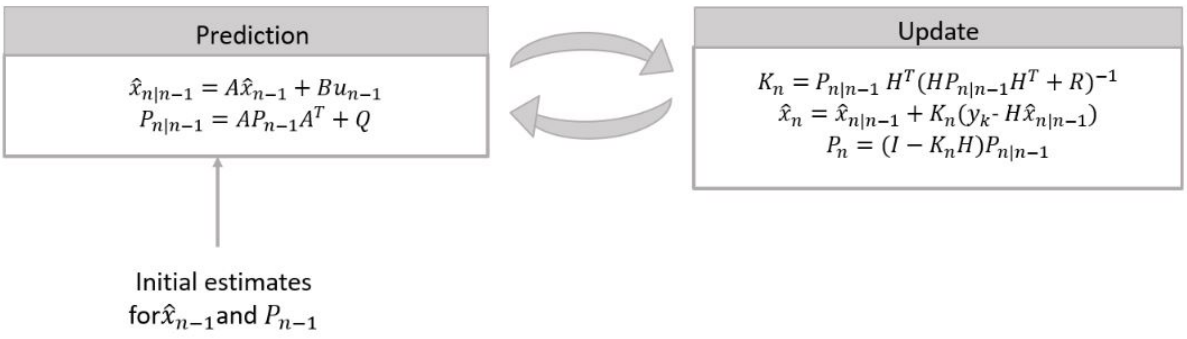

Figure 3.1: Kalman Filter Algorithm.

Extended Kalman Filter

The KF assumes that the system is linear, however real-world systems may be non-linear. The Extended Kalman Filter (EKF) addresses the filtering problem in case the system dynamics and observation equations are nonlinear. In other words, the EKF is an extension of the standard KF to nonlinear systems.

$$\begin{cases} y_n = h(x_n, w_n) \\ x_n = f(x_{n-1}, u_n) \end{cases} \tag{3.4}$$

where $f(.)$ is the state transition model applied to the previous state x_{n-1}, u_n and fw_n correspond to the process and observation noise which are assumed to be white, zero-mean, uncorrelated ($E[w_n {u_n}^T] = 0$) with associated covariance matrices $Q_n = E\{u_n {u_n}^T\}$ and $R_n = E\{w_n {w_n}^T\}$ respectively [3]. It is further assumed that the components of the noise processes are uncorrelated i.e., Q_n and R_n are diagonal. $h(.)$ is the observation model that maps state space into the observed space. The KF estimates the state x_n based on the knowledge of the system dynamics and the noisy measurements y_n.

The non-linearities of the system's dynamics are approximated by a linearized version of the non-linear system model around a desired reference point. The linear approximation near the desired reference point $(\hat{x}_n, \hat{w}_n, \hat{u}_n)$ will lead to the following linear estimates:

$$\begin{cases} y_n = h(\hat{x}_n, \hat{w}_n) + C_n(x_n - \hat{x}_n) + G_k(w_n - \hat{w}_n) \\ x_n = f(\hat{x}_{n-1}, \hat{u}_n) + A_n(x_{n-1} - \hat{x}_{n-1}) + F_k(u_{n-1} - \hat{u}_{n-1}) \end{cases} \tag{3.5}$$

where

$$\begin{aligned} A_n &= \frac{\partial f(x_n, \hat{u}_n)}{\partial x}|_{x=\hat{x}_n} & F_n &= \frac{\partial f(\hat{x}_n, \hat{u})}{\partial u}|_{u=\hat{u}_n} \\ C_n &= \frac{\partial h(x_n, \hat{w}_n)}{\partial x}|_{x=\hat{x}_n} & G_n &= \frac{\partial h(\hat{x}_n, \hat{w})}{\partial w}|_{w=\hat{w}_n} \end{aligned} \tag{3.6}$$

The EKF linearization is shown in Figure 3.2.

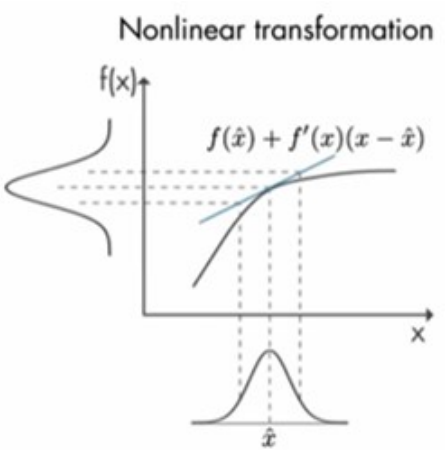

Figure 3.2: EKF linearizing a non-linear function around the mean of a Gaussian distribution.

The time update step of the Kalman filter algorithm obtains the predicted value of the state vector and the covariance of its error. The predicted state vector and the covariance of its error at time n are computed from propagating their corresponding values at time $n-1$ through the state dynamics as follows:

$$\begin{aligned} \hat{x}_{n|n-1} &= f(\hat{x}_{n-1}, u_{n-1}) \\ P_{n|n-1} &= A_{n-1} P_{n-1} A_{n-1}^T + Q_n \end{aligned} \tag{3.7}$$

where $\hat{x}_{n|n-1}$ is the predicted value of the state vector, $P_{n|n-1}$ is the covariance of the error of the predicted state vector given by $P_{n|n-1} = E[(\hat{x}_n - \hat{x}_{n|n-1})(\hat{x}_n - \hat{x}_{n|n-1})^T]$, and $E[.]$ is the expectation operator. Once the measurement vector is received, the measurement update step is used to compute the estimate of the state vector, $\hat{x}_n$ and the covariance of the error of the state vector, P_n, by applying corrections to the corresponding predicted values based

on the measurement obtained as follows:

$$
\begin{aligned}
K_n &= P_{n|n-1}C_n^T(C_nP_{n|n-1}C_n^T + G_nR_nG_n^T)^{-1} \\
\hat{x}_n &= \hat{x}_{n|n-1} + K_n(y_n - h(\hat{x}_{n|n-1}, w_n)) \\
P_n &= (I - K_nC_n)P_{n|n-1}
\end{aligned}
\tag{3.8}
$$

where K_n is the Kalman gain, and I is a diagonal matrix. Figure 3.3 offers a complete picture of the operation of the EKF.

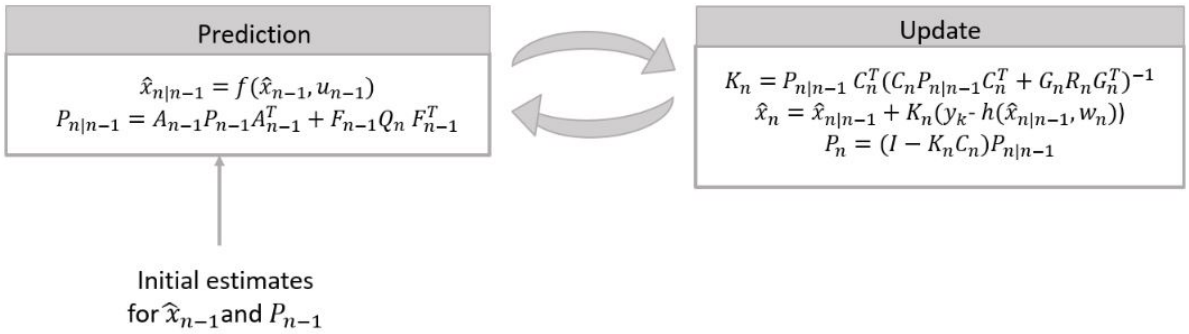

Figure 3.3: Extended Kalman Filter Algorithm.

3.3 Blind Source Separation (BSS)

The BSS methods assume that the abdominal signal is a mixture of independent signals, consisting of fECG, mECG, and noises [26].

3.3.1 Independent Component Analysis (ICA)

ICA is a mathematical technique for recovering unobserved source signals (components) from observed signal mixtures. Let us denote a matrix Let us denote the random observed vector $\mathbf{X} = [\mathbf{x_1}, \mathbf{x_2}, ..., \mathbf{x_n}]$ considered as observed signals which are assumed to be linear.

Instantaneous mixtures of the source signals are denoted by a matrix $\mathbf{S} = [\mathbf{s_1}, \mathbf{s_2}, ..., \mathbf{s_n}]$. We can present the relationship between X and S by the following equation:

$$\mathbf{X} = \mathbf{AS} \tag{3.9}$$

where matrix $\mathbf{A}$ represents a $n \times n$ mixing matrix and contains the mixture coefficient. The goal of ICA is to find the unmixing matrix $\mathbf{W}$ (i.e., the inverse of $\mathbf{A}$) that will give the matrix $\mathbf{Y}$-the best possible approximation of $\mathbf{S}$ by:

$$\mathbf{Y} = \mathbf{WX} \cong \mathbf{S} \tag{3.10}$$

For this purpose, a number of criteria can be considered on the basis of the maximization of non-gaussianity, maximum likelihood, and minimization of mutual information, to name a few [45]. Typically, ICA algorithms can be broken into several steps, including centering, whitening, and iterative algorithms. While the centering step is utilized to make the signal a zero-mean variable, whitening step is applied for transforming the observed signals so that the new processed observed signals are white (i.e., their components are uncorrelated and their variances equal to unity) [45]. The whitening step is necessary as it can significantly simplify the ICA problem. For iterative algorithm steps, there is a number of formulations for this procedure. For instance, the Joint Approximation Diagonalization of Eigenmatrices (JADE) algorithm was first developed as an application of blind identification in beamforming [66, 67] which is iterative with a defined number of iterations. The FastICA algorithm is considered to be the most popular method among ICAs due to its simplicity, convergence speed, and satisfactory results in numerous applications [45]. This algorithm is often used in 'real time' applications because of the possible parallel implementation. It converges quickly as it seeks the components one by one. FastICA uses simplified kurtosis for the independent component estimation, and the detail of this algorithm has been summarized in Figure 3.4. Another optimization algorithm is RobustICA. Compared with FastICA, RobustICA uses

a general kurtosis contrast function to maximize the non-gaussianity, as shown in Figure 3.5. The process of this method is described in [68]. Overall, using RobustICA has some advantages over FastICA, such as (1) pre-processing is not required which allows one to deal with all signal types; and (2) RobustICA uses an adaptive step size, ensuring that the weights converge to the actual convergence point, thus avoiding getting trapped as the former algorithm does.

Algorithm 1: FastICA

1. Pre-processing

- Centering $\quad x' = x - mean(x)$
- Whitening $\quad x' = ED^{-1/2}E^T x$

2. Weight update

- Choose random initial starting weight vector $\mathbf{w}$
- Let $\quad \mathbf{w}^+ = E\{\mathbf{x}g(\mathbf{w}^T\mathbf{x})\} - E\{g'(\mathbf{w}^T\mathbf{x})\}\mathbf{w} \qquad (*)$

with $\mathbf{x}$ is the centered and whitened data and g is the function that selects one of the following two functions

$$g_1 = tanh(a_1 u)$$
$$g_2 = u * exp(-u^2/2)$$

- Let $\quad \mathbf{w} = \mathbf{w}^+ / \| \mathbf{w}^+ \|$
- If not converged, go back to (*).
- Decorrelate if working with several units

$$\mathbf{w}_{p+1} = \mathbf{w}_{p+1} - \sum_{j=1}^{p} \mathbf{w}_{p+1}^T \mathbf{w}_j \mathbf{w}_j$$

$$\mathbf{w}_{p+1} = \mathbf{w}_{p+1} / \sqrt{\mathbf{w}_{p+1}^T \mathbf{w}_{p+1}}$$

3. Source extraction

$$y = \mathbf{w}^T \mathbf{x}$$

Figure 3.4: FastICA algorithm.

3.4 Template Subtraction

The main idea of TS is to regenerate mECG and then subtract it from aECG. Based on maternal QRS detection, we identify each mECG cycle $\underline{m}$ belonging to 0.25 seconds before and 0.45 seconds after maternal R peak positions with respect to the duration of the whole

Algorithm 2: RobustICA

1. No Pre-processing Required

2. Weight update

- Choose random initial starting weight vector **w**
- Let $w^+ = w + \mu_{opt} g$ (*)

$$g = \nabla_w K(w) = \frac{4}{E^2\{|y|^2\}} \left\{ \begin{array}{l} E\{y|^2\ y^* x|\} - E\{yx\}E\{y^{*2}\} \\ -\dfrac{(E\{|y|^4\} - |E\{y^2\}|^2)E\{y^* x\}}{E\{|y|^2\}} \end{array} \right\}$$

$$\mu_{opt} = argmax_{\mu}(|K(w + \mu_{\mu}\mathbf{g})|)$$

- Let $\mathbf{w} = \mathbf{w}^+ / \|\mathbf{w}^+\|$
- If not converged, go back to (*).
- Decorrelate if working with several units

$$\mathbf{w}_{p+1} = \mathbf{w}_{p+1} - \sum_{j=1}^{p} \mathbf{w}_{p+1}^T \mathbf{w}_j \mathbf{w}_j$$

$$\mathbf{w}_{p+1} = \mathbf{w}_{p+1} / \sqrt{\mathbf{w}_{p+1}^T \mathbf{w}_{p+1}}$$

3. Source extraction

$$y = \mathbf{w}^T \mathbf{x}$$

Figure 3.5: RobustICA algorithm.

cardiac cycle. The template maternal ECG (tECG) $\underline{t}$ then was formed by taking the average of all maternal ECG cycles, and the new mECG was obtained by replicating the $\underline{t}$ as shown in Figure 3.6. Another improved method based on the TS was utilized in this work, namely TSc. In this method, the template maternal ECG cycle $\underline{t}$ was scaled with a constant α. The scaling of $\underline{t}$ reduces the mismatch between the average and the actual mECG cycle $\underline{m}$, which is caused by the time-vary morphology of the mECG [69, 70]. The scaling constant a was based on the search for the last-mean square (LMS) e^2 error between $\underline{m}$ and $\underline{t}$, as shown in the following formula:

$$a = min \parallel \underline{t}.a - \underline{m} \parallel \tag{3.11}$$

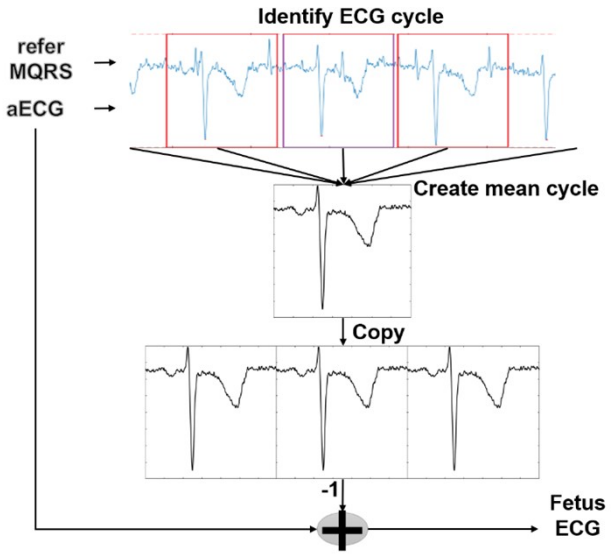

Figure 3.6: Template subtraction (TS)'s illustration for aECG.

3.5 TS and ICA combination

The combination of different methods could yield higher performance [71]. There are many ways of classifying the methods for extracting the fECG from the aECG mixture. The different combinations are denoted as follows (1) TS-ICA; (2) ICA-TS; and (3) ICA-TS-ICA.

Figure 3.7 illustrates the fQRS detection process with TS, ICA, and their combinations. First, the aECG signals were preprocessed to remove the baseline wander, power line noise, and high-frequency noise. Specifically, a notch filter with the cutoff frequency of 50 Hz was utilized to remove the power line noise while a high pass filter and a low pass filter were deployed to eliminate the baseline wander and high-frequency noise with the cutoff frequency of 10 and 99 Hz, respectively. Second, it should be noted that the mECG's amplitude is usually larger than other components in aECG. Thus, the Pan-Tompkin algorithm was implemented on four aECG signals, resulting in R peaks of mECG (mQRS detection) [72]. Third, the algorithms in the source separation block, which could be the TS method, ICA method, or combined methods, have been used. In the case of TS, as described in Section

2.2, after mQRS detection, a template mECG was produced. Subsequently, we subtract the aECG with the template mECG, resulting in four residuals. Finally, the Pan-Tompkin algorithm was used to detect fQRS. With the available fQRS reference annotations, the channel having the highest F1 score would be chosen. In the case of ICA, three different ICA methods (i.e., JADE, FastICA, and RobustICA) were utilized in source separation. After applying ICA, the output would be fECG, mECG, and two other noise signals. The reference mQRS would be used to select the mECG channel in the output. The Pan-Tompkin algorithm was then utilized for other channels (i.e., fECG and two other noise signals). Finally, the fECG channel was chosen based on a smoothing indicator (SMI). Specifically, the SMI was defined as the number of occurrences, over each-minute segments, where the absolute value of the change in instantaneous heart rate is more than 29 beats per minute [73]. This threshold was empirically determined on the data and which channels had the lowest SMI, was referred to fECG channel.

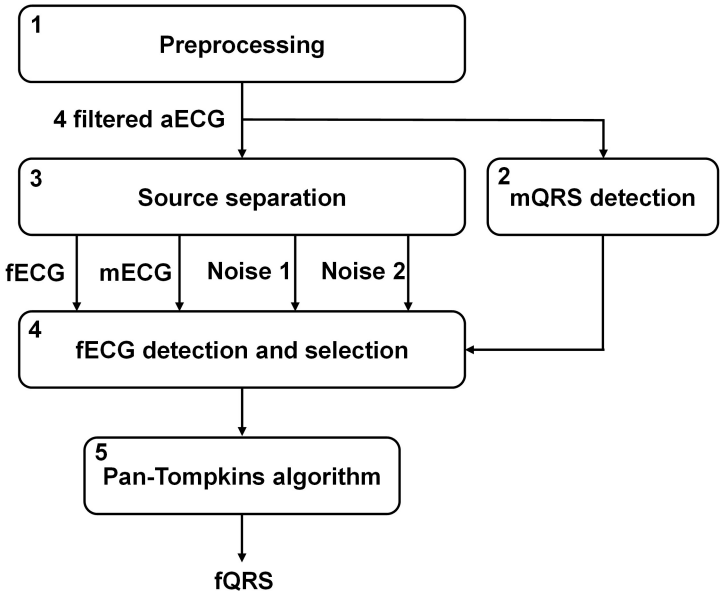

Figure 3.7: fQRS detection process: (1) Preprocessing step with notch filter, high pass filter and low pass filter utilized; (2) The Pan-Tompkins algorithms applied for mQRS detection used to create a template mECG and for channel selection in independent component analysis (ICA) method; (3) Source separation includes different approaches (TS, ICA and its hybrid). For ICA and the hybrid method, the extracted signals contain 4 signals (i.e., fECG, mECG and two noise signals; (4) Using mQRS detection from (2) as a criterion for fECG selection; (5) The Pan-Tompkins algorithm applied for fQRS detection.

Chapter 4

Database and Evaluation Criteria

4.1 Introduction

This chapter introduces the online and own databases used in the thesis. The statistical measures used for evaluating the non-invasive fetal electrocardiogram (NI-fECG) extraction methods are also presented. Furthermore, the modified data with Gaussian and motion noise added, mimicking practical scenarios were used to generate the artificial databases developed in the context of this thesis is also described.

4.2 Data

4.2.1 Online Data: PhysioNet 2013 Challenge databank

The data were taken from the PhysioNet 2013 Challenge databank which consists of a collection of one-minute abdominal ECG recordings (aECG) [74]. Each recording includes four noninvasive abdominal signals. The data were obtained from multiple sources using a

variety of instrumentation with differing frequency response, resolution, and configuration; although in all cases they are presented as 1000 samples per signal per second. Set A includes noninvasive fetal ECG signals, as well as the reference annotations for them which make validating the methods possible. This set contains 75 records, excluding a number of recordings (a33, a38, a47, a52, a54, a71, and a74) that had inaccurate reference annotations [71]. In each case, reference annotations marking the locations of each fetal QRS complex were produced, usually with reference to a direct fECG signal, acquired from a fetal scalp electrode. The reference annotations are produced by a team of experts manually.

4.2.2 Own Clinical Data

We developed the gen-2 'fetal monitoring patch' containing non-contact electrodes (NCEs), electronics, and secure communication with a smart device via Blue-tooth Low Energy (BLE) [46] (Figure 4.1). The compact patch is 4 inches long and unobtrusive, thus, it can be integrated on or inside maternity garments. The gen-2 patch has one single NCE channel to collect the aECG of the pregnant subject. The collected data are sent to an Android app connected to a cloud server for analytics. The system was validated on 10 pregnant women between 28 and 34 weeks of gestation in the University of California, Irvine (UCI) Medical Center. Each subject was resting on a chair during recording, and a maternity belt with the fECG patch attached is worn so that the NCEs are located in the abdominal area below the navel. The data were then collected in 5 minutes for each posture. More details are described in our previous paper [14]. All clinical recordings were collected anonymously under Institutional Review Board (IRB) approval 2020-6342 at the UCI.

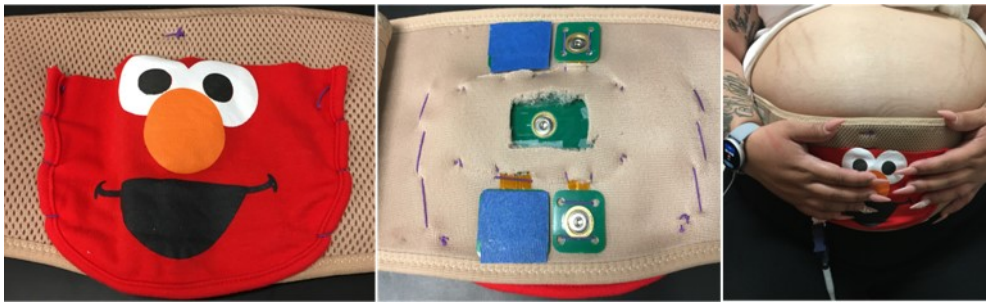

Figure 4.1: The fetal monitoring patch is a self-administered device consisting of non-contact electrodes, electronics, and BLE worn by the pregnant woman. The wireless fetal heart monitoring prototype in use at UCI Medical Center.

4.2.3 Online Data: MIT-BIH Noise Stress Test Database

Generally, all algorithms under development would be evaluated using reliable and open online databanks of clean ECG signals. Our experiments use the MIT-BIH Noise Stress Test Database includes twelve-half hours of ECG recordings and three-half hours of ECG with typical noise such as baseline wander, muscle artifact, and electrode motion artifact [75]. Clean ECG signals were used from the MIT-BIH Arrhythmia Database (102, 108, 121, 122, 215, 220, 232, 118, and 119), and each dataset was calibrated at six noise levels based on different signal-to-noise ratios (SNR) from -6 to 24 dB at 360 samples per second.

4.2.4 Modified Online Data

Modified abdominal signals with Gaussian noise added

With different practical scenarios in fetal/maternal ECG measurement, various kinds of noise appear. According to the Central Limit Theorem, those noises tend toward a normal distribution. Therefore, Gaussian noise with different dB has been added to the data to mimic the real scenarios. Specifically, the normally-distributed random noises are generated by randn function in MATLAB with the lowest amplitude ranging from -4 µV to 4 µV, which

is denoted as noise level 0. Then, different noise levels would be increased by multiplying with constant numbers divisible by 3 (i.e., 3, 6, 9, 12, 15, 18, and 21).

Modified abdominal signals with motional artifacts added

The dataset was obtained in the clinical setting where motion noise was mostly avoided because the subjects were in a resting position, so the movement artifacts should be added to the data for practical applications. We attempted to generate a realistic motion noise. First, the ECG data were recorded from a healthy subject in different types of activities such as walking. For ECG recording, the OpenBCI Cyton board (OpenBCI, Brooklyn, NY) was used with 2 of its default electrodes. The board communicates wirelessly to a computer. Since the amplitude of the noise is an important factor, normalization had been used for all signals to reinsure aECG and the motion noise has realistic amplitudes. For extracting motion noise, Extended Kalman Filter was employed as shown in Figure 4.2. First, the acquired data should be normalized between -1 and 1, and then by using EKF, motion noise and filtered ECG data are achieved. In the second step, for adding the motion noise to aECG, the aECG data should be normalized with the same threshold. In the last step the motion noise is added to the normalized aECG (Figure 4.3).

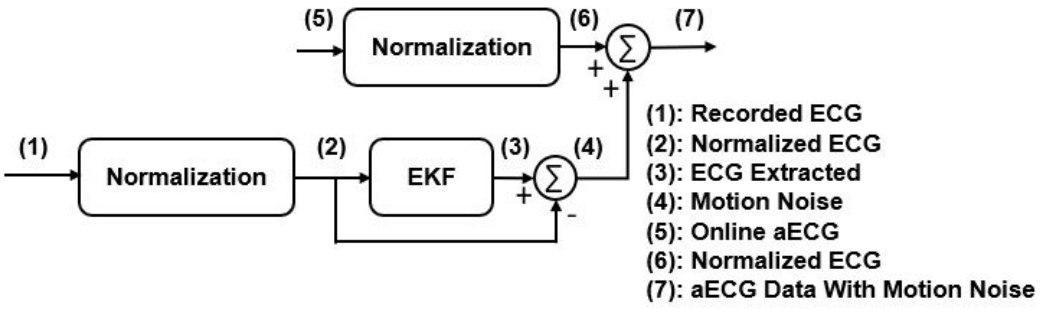

Figure 4.2: Implementation of motion noise generation procedure.

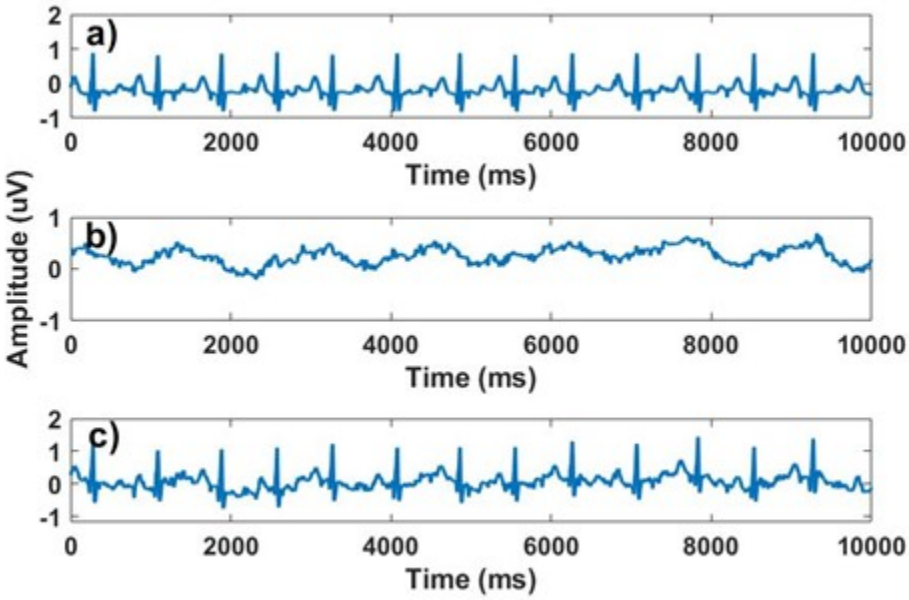

Figure 4.3: Illustration of applying noise to record a01 motion, (a) Normalized a01 record, (b) Generated motion noise, (c) a01 with added motion noise artifact.

Modified ECG signals with motional artifacts added

When an ECG signal is recorded in daily life, it would be contaminated with many kinds of noise, such as motion artifacts. Unfortunately, the online dataset collected in the clinical setting is the ideal resting position with minimal motion artifacts. Therefore, here, we added the motion noise to the online clean dataset to have a better realistic scenario in our experiments. The ECG data were recorded using the OpenBCI Cyton board (OpenBCI, Brooklyn, NY, USA) from healthy subjects during daily activities. Next, we normalized the recorded data to reinsure ECG and motion noise have realistic amplitudes. The EKF was employed to extract motion artifact noise. Then, ECG data should be normalized with the same threshold; before adding the motion noise to the new ECG. The generation process is also described in 4.2.4.

4.3 QRS detection

The Pan-Tompkin algorithm is one of the most popular methods in real-time approaches. Jiapu Pan, and Willis Tompkin developed this algorithm in 1985[**?**]. The algorithm utilized the signal features such as amplitude, slope, and width of each integrated window to detect the QRS complex. To be brief, this algorithm consists of two main steps; (1) pre-processing, (2) decision. The detail of this algorithm has been summarized in the following.

4.3.1 Pre-Processing

In general, the pre-processing can be divided into four stages; (1) Filtering, (2) Derivative, (2) Squaring, and (2) Moving Window Integration (MWI).

Filtering

The band-pass filter is used to reduce high-frequency noise such as interference in T- waves, Power Line Interference, and low-frequency noise such as muscle noise and baseline wander. The band-pass filter is obtained by cascading the low-pass filter and high-pass filter with cut-off frequencies 4 Hz and 15 Hz.

Derivative

To gain information about the slope of the QRS complex, the derivative is applied to the filtered signal. In this stage, high slope features are preserved. The T-waves and P-waves are suppressed in the derivative stage due to their low slope.

Squaring

The signal after the derivative process is squared because all components of the signal appear positive. The higher value in the squared signal represents the QRS complex. The squaring function by amplifying nonlinearly makes QRS complex diagnosis easier.

Moving Window Integration (MWI)

To gain information about the R-peak slope and waveform features, the MWI is used. The width of the integrated window must be matched with a QRS complex width.

4.4 Comparison Criteria

4.4.1 QRS detection accuracy

The performance of the extraction methods is assessed by comparing the beat-to-beat length of the extracted fECG QRS complex and the corresponding annotated data. According to the American National Standards Institute/ Association for the Advancement of Medical Instrumentation (ANSI/AAMI) guideline, *Sensitivity* (Se), *Positive Predictive Value* (PPV), and the accuracy measure ($F1$ score) which is the harmonic mean of PPV and Se, were used for assessment. The Se tells how accurate an algorithm is at finding the true fetal QRS. The PPV presents the performance of the algorithm at identifying true FQRS out of

all the detections. These statistical indices are computed as follows:

$$Se = \frac{TP}{TP + FN} \tag{4.1}$$

$$PPV = \frac{TP}{TP + FP} \tag{4.2}$$

$$F1 = 2.\frac{PPV.Se}{PPV + Se} = \frac{2\,TP}{2\,TP + FN + FP} \tag{4.3}$$

where TP, FP, and FN are true positive (correctly identified QRS), false positive (wrongly detected QRS), and false negative (missed QRS) detections respectively.

4.4.2 Noise reduction performance

To evaluate the performance of denoising algorithms in Chapter 6, the improvement in SNR before and after denoising, the root mean square error (RMSE), the Percentage Root Difference (PRD), and the correlation coefficient between the denoised and the clean signal are calculated.

$$SNR = 10\,log(\frac{\sum_{i=1}^{n} x^2(n)}{\sum_{i=1}^{n}(x(n) - y(n))^2}) \tag{4.4}$$

$$RMSE = \sqrt{\frac{1}{n}\sum_{i=1}^{n}(x(n) - y(n))^2} \tag{4.5}$$

$$PRD = \sqrt{\frac{\sum_{i=1}^{n}(x(n) - y(n))^2}{\sum_{i=1}^{n} x^2(n)}} \times 100 \tag{4.6}$$

where $x(n)$, and $y(n)$ are the original and the denoised signal respectively.

4.5 Summary

This chapter presented the databases used in this thesis. A total of four databases for the experiments presented in Chapters 5, 6, 7, and 8 . The statistical parameters which assess the detection of the QRS complex waveform of the fECG and the performance of denoising algorithms were used which were also presented in this chapter. Finally, the Pan-Tompkin algorithm, used for fetal QRS detection, was introduced.

Chapter 5

A Fetal ECG Monitoring System Based on the Android Smartphone

5.1 Introduction

Some home-based fECG systems were developed and introduced; nevertheless, they are bulky, costly, and intrusive, and thus have not been widely used. Continuous fECG monitoring has remained a challenging problem in the research community [33]. Our group has developed the gen-2 'fetal monitoring patch' containing non-contact electrodes (NCEs), electronics, and secure communication with a smart device via Bluetooth Low Energy (BLE) [46, 65]. The compact patch is 4 inches long and unobtrusive, thus, it can be integrated on or inside maternity garments. The gen-2 patch has one single NCE channel to collect the aECG of the pregnant subject. This abdominal patch is made of flexible and stretchable polymer that can be worn with any user, or embedded inside clothes, thus bringing comfort and versatility. The entire system is shown in Figure 5.1. Prior to the extraction of the fECG and mECG, the abdomen signal should be processed to remove the baseline wander (drift).

Figure 5.1: Fetal ECG monitoring system overview.

The wavelet denoising method was used as reported in our previous work [76]. Figure 5.2 shows an example of this technique applied to an NCE ECG signal recorded using one of our prototypes.

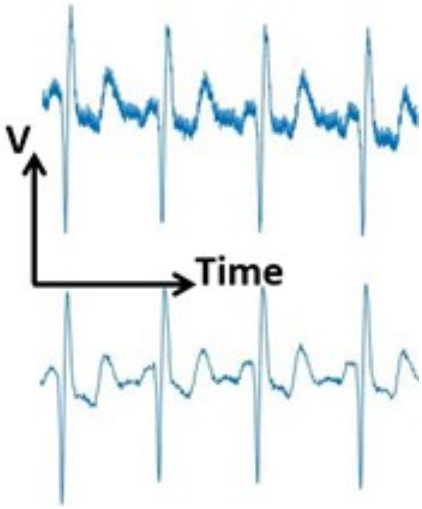

Figure 5.2: The NCE ECG obtained by our system and an ECG denoising example.

In this chapter, a home-based fetal and maternal monitoring system, including a fetal patch, a mobile application, and a cloud server is designed and implemented (Figure 5.3).

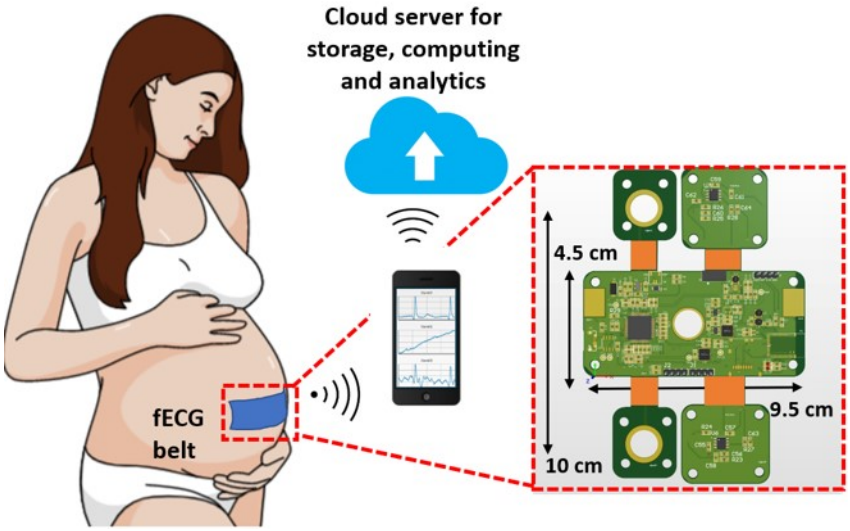

Figure 5.3: Fetal ECG monitoring patch and system.

5.2 Methods and Implementation

We developed hardware and software components to create a remote prenatal care system. The abdominal ECG signals are collected by a wearable patch, and then the collected data are sent to the Android app via BLE communication. The pre-processing and extraction algorithms are performed through the connected cloud server from the app to separate the fECG and mECG. Then, fHR calculation is performed to assess the performance of the device. Finally, the fECG and fHR are displayed in real-time on the app. Users will be warned to visit the hospital when a critical event, or better yet, a pre-critical event, occurs.

5.2.1 The fetal patch

The patch is made of a flexible-rigid printed circuit board with dimensions of 4.5 cm × 9.5 cm. Two wings having electrodes measured 10 cm apart are designed with a flexible material (highlighted in orange – Figure 5.3), which increases the contact surface between the electrode and abdominal area. It contains two types of electrodes (i.e., Ag/AgCl wet electrode

and non-contact electrode) for validation and comparison. While the wet electrodes can provide high signal to noise ratio (SNR) by having the electrolyte gel, it was known to cause skin irritation for long-term measurement [77]. Thus, we deployed the NCE as an alternative on the patch. The dual-channel design is to characterize and compare the performance of the contact and non-contact approaches. The patch's circuitry comprises an ADS1299 chip (Texas Instrument) with 24-bit analog-to-digital converter specifically designed for biomedical signal measurement and a system-on-chip nRF82832 (Nordic Semiconductor, Trondheim, Norway) powered with Arm Cortex-M4 CPU running at 64 MHz. The nRF5282 is used to transmit data from ADS1299 to the Android application through BLE.

5.2.2 Fetal ECG Extraction Algorithm

fECG extraction algorithms can be classified into three groups: blind source separation (BSS), template subtraction, and filtering techniques. The BSS methods assume that the abdominal signal is a mixture of independent signals, consisting of fECG, mECG, and noises [26]. In our first-generation system, we utilized the least-mean square adaptive filtering [65]. Further, we implemented the BSS method via the independent component analysis (ICA), FastICA and RobustICA, and validated and compared them with the online data [46]. In our recent report, we implemented and tested various techniques, including Extended Kalman Filter (EKF), template subtraction (TS), ICA and their combination using the PhysioNet 2013 Challenge data bank as well as the data with added Gaussian and motion noise, to mimic daily life situations with wearable devices [13].

Among these, EKF is a powerful approach for single-channel fECG extraction [34]. The celebrated Kalman Filter (KF) is an optimal algorithm for estimating parameters of linear and Gaussian dynamic models [78]. EKF is used for nonlinear problems, which is based on local linearization of the nonlinear model by using the Jacobian operator [79]. The EKF

algorithm flow is shown in Figure 5.4. The data obtained in the home-based monitoring is contaminated with various kinds of noise, which motion noise is high level, so the preprocessing algorithm is indispensable for accurate fECG extraction in practical applications. First, the baseline wander and noise will be removed by using the lowpass filter, a notch filter, and a Wavelet filter. Next, the EKF will be employed to extract mECG. Then mECG will be removed by subtracting it from the processed signal. The output of this step is fECG along with noise, and then another EKF will be used to extract fECG.

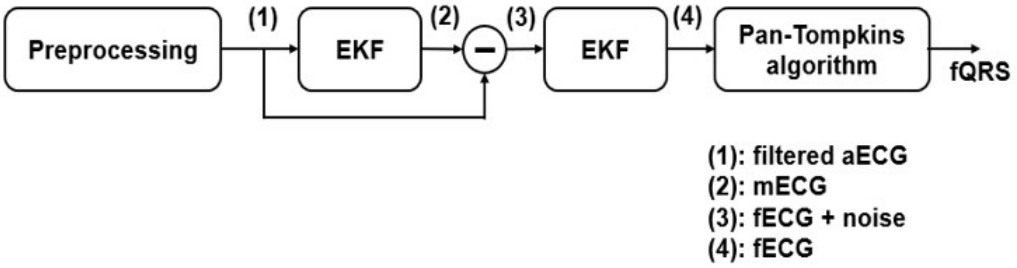

Figure 5.4: Fetal ECG monitoring patch and system.

5.2.3 Android Smartphone App Software

We developed an Android smartphone application in Java that connects to the patch via BLE communication for data collection, displaying, and logging. Through BLE protocols, the app connects to the fetal patch and reads in multiple data channels at a rate of 500 Hz. After accumulating at least 1,000 data points, the input data are sent to a cloud server to extract the fetal and maternal ECG through the algorithm described in Section 5.2.2. This would provide sufficient data to detect peaks and extract the fECG with higher accuracy. The results will start appearing on the application interface after 10 seconds of initially starting in the form of dynamic graphs as well as numerical values for the fHR. The user can disconnect the patch at any time and save the raw data with associated time points they are received in the application to a text file with a customizable name in the phone's external

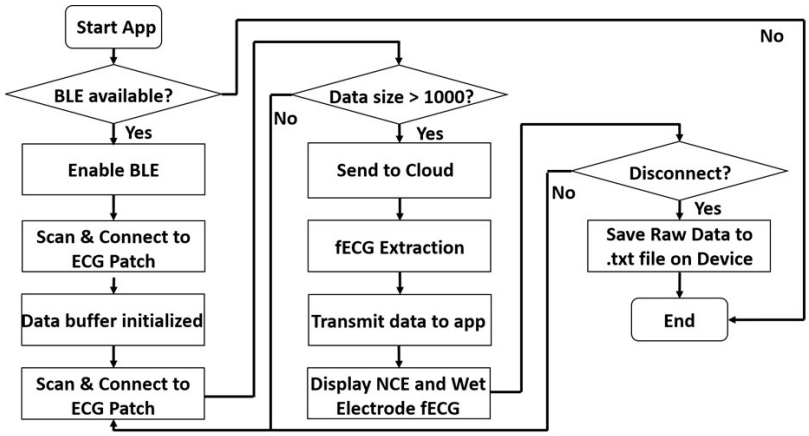

Figure 5.5: Android application operation flow chart.

storage. The results of the algorithm will also be saved in the cloud. The user also can load past text files to view the raw data and process fECG and fHR. This process is depicted in the flow chart in Figure 5.5.

5.3 Results

5.3.1 Algorithm Validation

The EKF algorithm described in Section 5.2.2 is implemented on mobile app for real-time fECG extraction (Figure 5.6). To evaluate the accuracy of the mobile app, we tested it with the PhysioNet 2013 Challenge databank which is described in 4.2.1. To implement the mobile app, the MATLAB code must be converted to Java. In this conversion, because all functions must be rewritten, the application may not have the same accuracy as MATLAB code. The mobile app was compared in terms of the F1 score and evaluated against MATLAB. F1 score is an accuracy measure (more details on the F1 score can be found in Section 4.4.1). Table 5.1 presents the average F1 score results in the 68 aECG records using the mobile app and MATLAB code. It can be seen that the mobile app is reliable as the results are comparable

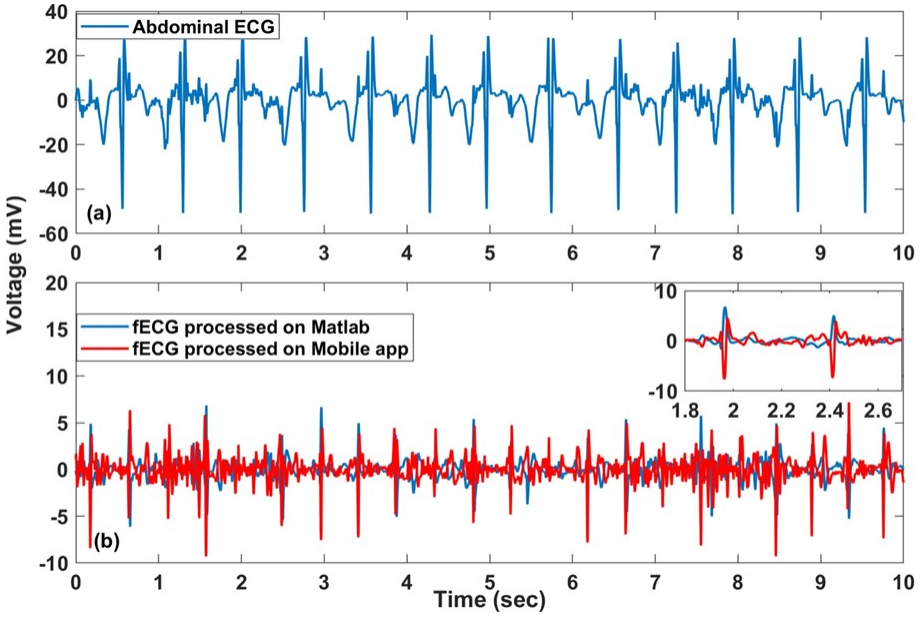

Figure 5.6: Results of fetal ECG Extraction by using the Mobile app and MATLAB. (a) A signal from PhysioNet 2013 Challenge databank; and (b) the fECG signal on Mobile app and MATLAB.

Table 5.1: Average F1 score (%) with mobile app and MATLAB code for all records

	Mobile App	MATLAB
F1 Score	84.8	86.7

to that of MATLAB.

5.3.2 Device Validation

The fetal patch was first validated on a healthy subject in different postures (e.g., sitting, walking, and standing). Figure 5.7 describes the patch setup and mobile application user interface. Specifically, two flexible belts were used to attach the patch to the abdominal area. The volunteer was asked to perform different activities such as sitting on a chair, walking slowly, and standing. The mobile application was then turned on connecting with the patch. The index graph showed the data transmit package, checking if there is any data lost during

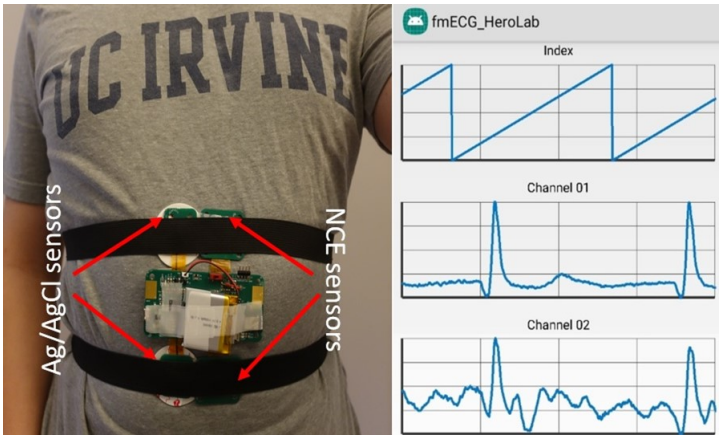

Figure 5.7: The fetal patch setup and experiment.

the transmission. The data were then collected in 5 minutes for each posture. Figure 5.8 illustrates the ECG data (plotted in the first 20 seconds) from the first experiment. It can be seen that the ECG signal in the sitting position is clean and more stable than those recorded in standing and walking positions. Especially, motion artifacts were found in the signal with walking position.

5.3.3 Entire System Validation

The entire system was further validated on 10 pregnant women between 28 and 34 weeks of gestation in the UCI Medical Center (see Section 4.2.2 for more details). The patch was embedded inside a maternity belt. The pregnant subjects were asked to perform a transabdominal ECG recording within 5 minutes. Each subject was laid on the chair and the belt with the fetal patch was attached to the abdominal area. The recorded data are sent to the smart device app via secure BLE communication. The real-time monitoring android smartphone app software is depicted in Figure 5.9. Figure 5.9 illustrates the collected ECG and processed fECG of a pregnant woman. The obtained ECG was filtered to remove DC noise and interference and applied to the fECG extraction algorithm as described in 5.2.2. As can be seen, our system can successfully collect the abdominal ECG and extract the

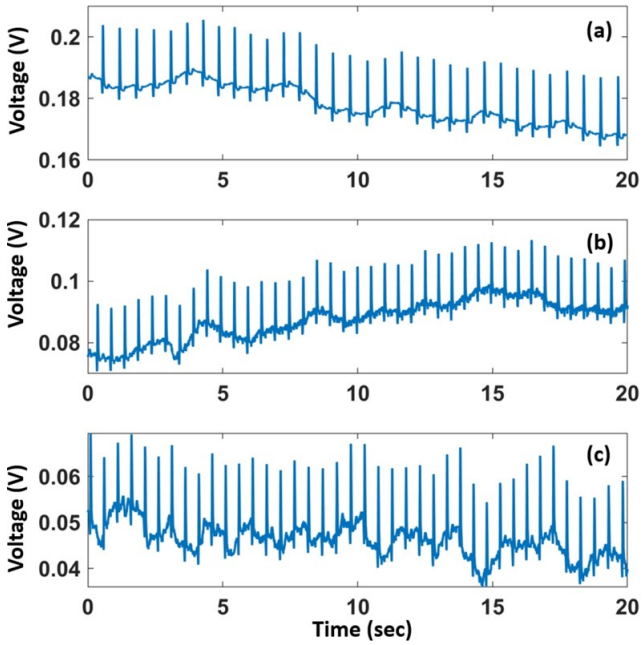

Figure 5.8: ECG signals recorded from the patch: (a) sitting position, (b) standing position, (c) walking position.

peaks of fECG (highlighted in red in Figure 5.10c). For this pregnant woman, the fHR is measured at 100 beats per minute which is normal for this stage of pregnancy.

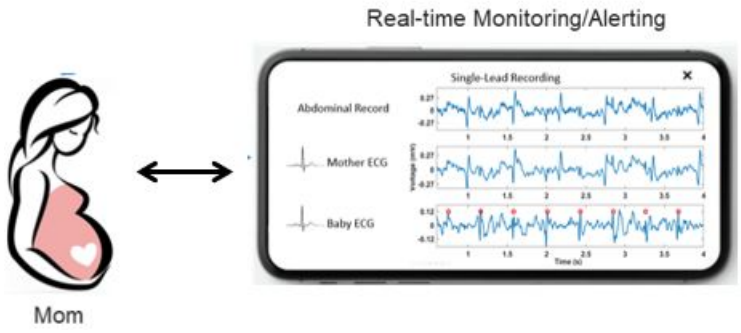

Figure 5.9: Real-time monitoring/altering android smartphone app software.

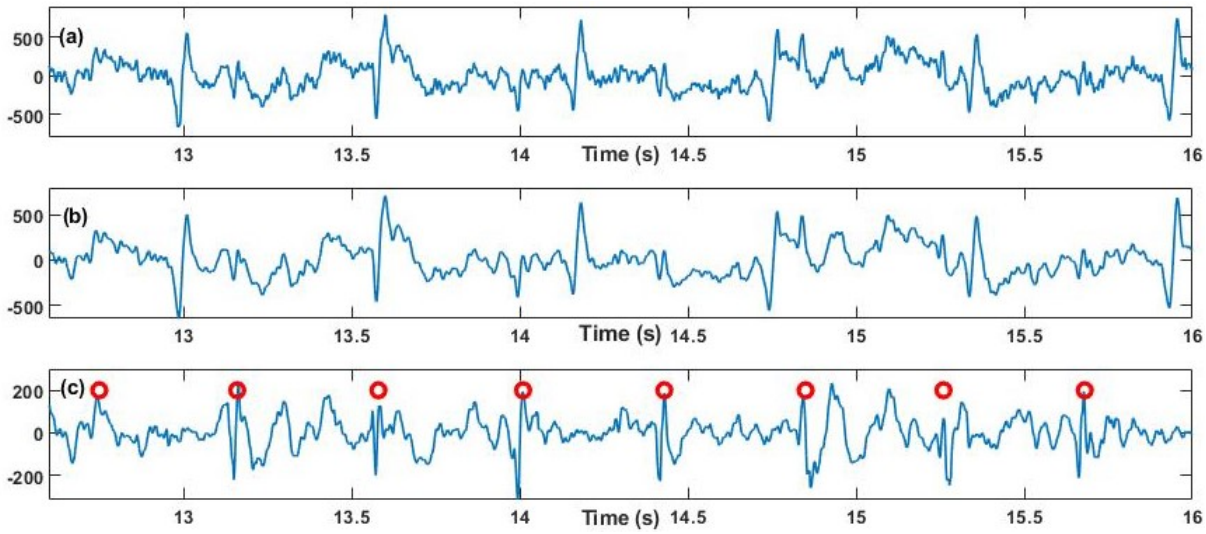

Figure 5.10: Results of fetal ECG extraction by using the Android application. (a) recorded data from maternal abdominal; (b) filtered data; and (c) Fetal ECG extracted and fetal QRS detected.

5.4 Discussion

We have developed a fetal ECG monitoring device and extraction algorithms implemented on an Android smartphone which is capable of providing real-time and continuous fetal monitoring. We extensively investigated the use of the developed device for signal acquisition, which holds promise to be widely used as it can be unobtrusive bring integrated inside garment. We rigorously conducted several experiments to validate the operation of all components. The Android smartphone application was compared in terms of the F1 score and evaluated against offline processing using MATLAB. The results indicate that the mobile app is reliable on its own. The entire system was tested with 10 pregnant subjects, demonstrating its feasibility. Specifically, the aforementioned device has been successfully applied to collect and extract fECG from aECG, and the efficacy of the proposed system has been carried out with real-time data recordings on pregnant subjects. Our Android application provides graphical and numerical information of fECG to assess fetal wellbeing. The fHR was calculated, and the fECG and fHR were displayed in real-time. Examination of patterns

and fHR obtained would indicate the need to take the appropriate medications during labor.

Chapter 6

Novel Approaches for Non-Invasive Fetal ECG Extraction

6.1 Introduction

The fECG would provide valuable information that could help to deliver better fetal monitoring as well as assist clinicians in making more appropriate and timely decisions during labor. We have been developing abdominal patch devices and systems for the acquisition and extraction of fECG in Chapter 5 [13, 46, 65]. As we aimed to make the device compact and unobtrusive, a single recording channel is desired for saving space; consequently, fECG extraction is almost impossible, especially with the presence of motion noise [33].

In chapters 3 and 8 , we reviewed and implemented the fECG extraction methods and its challenging issues. It was noted that in the current chapter we are interested in improving the signal processing aspects of these problems, in order to facilitate the extraction of fECG signals.

fECG extraction methods based on variants of the Kalman filtering technique are used widely. The original Kalman Filter (KF) was designed by R. E. Kalman for linear models and the noises involved are additive [78]. For nonlinear problems, Extended Kalman Filter (EKF) is used, which is based on local linearization of the nonlinear model using the Jacobian [79]. G. Evensen introduced the EnKF [80]. In this chapter, a newly developed approach for Non-invasive fECG extraction is presented. The proposed approach is based on using the Ensemble Kalman filter (EnKF) to extract f/m ECG which exhibits robust and efficient performance for many signal processing problems. Currently, there is no approach available to extract fetal characteristic waves.

6.2 Theory and Method

6.2.1 Review of Extended Kalman Filter

The EKF is a powerful approach for single-channel fECG extraction [34]. The celebrated KF is an optimal algorithm for estimating parameters of linear and Gaussian dynamic models [78]. EKF is used for nonlinear problems, which is based on local linearization of the nonlinear model by using the Jacobian operator [79]. Almost all real-life systems are non-linear and must be linearized before being estimated using a KF [81].

$$\begin{cases} y_n = h(x_n, w_n) \\ x_n = f(x_{n-1}, u_n) \end{cases} \tag{6.1}$$

where $h(.)$ is the observation function that maps state space into the observed space. $f(.)$ is the state transition function that describes the evaluation of the state variable x_n, u_n and w_n denote the process and observation noises and y_n is observation vector [52].

By calculating the Jacobian of $f(.)$ and $h(.)$ around the estimated state, this problem of

non-linearity is solved by EKF. The calculation of Jacobian yields a trajectory of the model function centered around the state.The linear approximation near a desired reference point $(\hat{x}_n, \hat{w}_n, \hat{u}_n)$ will lead to the following linear estimates:

$$\begin{cases} y_n = h(\hat{x}_n, \hat{w}_n) + C_n(x_n - \hat{x}_n) + G_k(w_n - \hat{w}_n) \\ x_n = f(\hat{x}_{n-1}, \hat{u}_n) + A_n(x_{n-1} - \hat{x}_{n-1}) + F_k(u_{n-1} - \hat{u}_{n-1}) \end{cases} \tag{6.2}$$

The EKF is described in detail in Section 3.2.

6.2.2 Ensemble Kalman Filter (EnKF)

EnKF is a variant of the celebrated Kalman filter used to estimate time-varying parameters in problems that arise in various disciplines [82]. It is applicable for problems that can be represented as dynamic systems and formulated in a state-space model with unknown time-varying state parameters. When the state-space model of the system is linear and Gaussian, the optimal estimate of the state parameters can be obtained using the Kalman filter [83]. However, when the problem is nonlinear or non-Gaussian, other variants of the Kalman filter, such as the EnKF, are used to obtain close-to-optimal solutions [84]. Our EnKF algorithm is developed by considering a Bayesian filtering framework and formulating the fECG extraction problem as a dynamic system whose state and measurement equations are represented in a state-space form. The dynamic model is adopted from the models proposed by McSharry et al. [85] and later discretized by Sameni [34].

Suppose the unknown time-varying state vector of a dynamic state-space model is denoted by $\mathbf{x_n} \in R^{D_x}$ where $n = 1, 2, \ldots, N$ represents time instants and D_x represents the dimension of $\mathbf{x_n}$. We assume that $\mathbf{x_n}$ has a Markovian property, and its evolution is given by:

$$\mathbf{x_n} = f_n(\mathbf{x_{n-1}}) + \mathbf{u_n} \tag{6.3}$$

where $f(.)$ represents a state function which, in general, is nonlinear, and $\mathbf{u_n}$ denotes the state noise vector with a known probability density function (pdf). Furthermore, the observation equation of the state-space model is given by:

$$\mathbf{y_n} = h_n(\mathbf{x_n}) + \mathbf{w_n} \tag{6.4}$$

where $\mathbf{y_n} \in R^{D_y}$ denotes the measurement vector obtained at time n, D_y represents the dimension of the vector D_y, and $\mathbf{w_n}$ denotes the measurement noise vector whose pdf is assumed known.

Given the state-space model (1) and (2), our objective is to make a sequential estimate of the evolution of the state vector $\mathbf{x_{1:n}} = \mathbf{x_1}, \ldots, \mathbf{x_n}$ in real-time as the measurement vector denoted by $\mathbf{y_{1:n}} = \mathbf{y_1}, \ldots, \mathbf{y_n}$ becomes available.

The Ensemble Kalman filter is a variant of the Kalman filter where the state error statistics are approximated using the Monte Carlo method. Recall that if the state equation (1) and the measurement equation (2) are linear, and the state noise $\mathbf{u_n}$ and measurement noise $\mathbf{w_n}$ are Gaussian, the optimal estimate of the state vector can be analytically obtained using Kalman filter. To understand the EnKF, let us review the Kalman filter algorithm's two steps: the time update and the measurement update. For convenience, we rewrite the state and measurement equations for a linear and Gaussian system as follows:

$$\begin{cases} \mathbf{y_n} = \mathbf{H}\mathbf{x_n} + \mathbf{w_n} \\ \mathbf{x_n} = \mathbf{F}\mathbf{x_{n-1}} + \mathbf{u_n} \end{cases} \tag{6.5}$$

where $\mathbf{F}$ is a $D_x \times D_x$ matrix, $\mathbf{H}$ is a $D_y \times D_x$ matrix, and $\mathbf{u_n}$ and $\mathbf{w_n}$ are zero-mean Gaussian probability densities with covariances $\mathbf{Q_u}$ and $\mathbf{Q_w}$, respectively.

The time update step of the Kalman filter algorithm obtains the predicted value of the state

vector and the covariance of its error. The predicted state vector and the covariance of its error at time n are computed from propagating their corresponding values at time $n-1$ through the state dynamics as follows:

$$\begin{aligned} \hat{\mathbf{x}}_{\mathbf{n|n-1}} &= \mathbf{F}\hat{\mathbf{x}}_{\mathbf{n-1}} \\ \mathbf{P}_{\mathbf{n|n-1}} &= \mathbf{F}\mathbf{P}_{\mathbf{n-1}}\mathbf{F}^{\mathbf{T}} + \mathbf{Q}_{\mathbf{u}} \end{aligned} \tag{6.6}$$

where $\hat{\mathbf{x}}_{\mathbf{n|n-1}}$ is the predicted value of the state vector, $\mathbf{P}_{\mathbf{n|n-1}}$ is the covariance of the error of the predicted state vector given by $\mathbf{P}_{\mathbf{n|n-1}} = E[(\hat{\mathbf{x}}_{\mathbf{n}} - \hat{\mathbf{x}}_{\mathbf{n|n-1}})(\hat{\mathbf{x}}_{\mathbf{n}} - \hat{\mathbf{x}}_{\mathbf{n|n-1}})^T]$, and $E[.]$ is the expectation operator. Once the measurement vector is received, the measurement update step is used to compute the estimate of the state vector, $\hat{\mathbf{x}}_{\mathbf{n}}$ and the covariance of the error of the state vector, $\mathbf{P}_{\mathbf{n}}$, by applying corrections to the corresponding predicted values based on the measurement obtained as follows:

$$\begin{aligned} \mathbf{K}_{\mathbf{n}} &= \mathbf{P}_{\mathbf{n|n-1}}\mathbf{H}^{\mathbf{T}}(\mathbf{H}\mathbf{P}_{\mathbf{n|n-1}}\mathbf{H}^{\mathbf{T}} + \mathbf{Q}_{\mathbf{w}}) \\ \hat{\mathbf{x}}_{\mathbf{n}} &= \hat{\mathbf{x}}_{\mathbf{n|n-1}} + \mathbf{K}_{\mathbf{n}}(\mathbf{y}_{\mathbf{n}} - \mathbf{H}\hat{\mathbf{x}}_{\mathbf{n|n-1}}) \\ \mathbf{P}_{\mathbf{n}} &= (\mathbf{I} - \mathbf{K}_{\mathbf{n}}\mathbf{H})\mathbf{P}_{\mathbf{n|n-1}} \end{aligned} \tag{6.7}$$

where $\mathbf{K}_{\mathbf{n}}$ is the Kalman gain, and $\mathbf{I}$ is a diagonal matrix. We note that the Kalman gain can be expressed as

$$\mathbf{K}_{\mathbf{n}} = \mathbf{P}_{\mathbf{xy,n}}\mathbf{P}_{\mathbf{yy,n}}^{\mathbf{-1}} \tag{6.8}$$

where $\mathbf{P}_{\mathbf{xy,n}}$ is the cross-covariance of the error of $\hat{\mathbf{x}}_{\mathbf{n|n-1}}$ and $\mathbf{y}_{\mathbf{n}}$, and $\mathbf{P}_{\mathbf{yy,n}}$ is the covariance of the error of $\mathbf{y}_{\mathbf{n}}$. These covariances are given by:

$$\begin{aligned} \mathbf{P}_{\mathbf{xy,n}} &= E[(\hat{\mathbf{x}}_{\mathbf{n}} - \hat{\mathbf{x}}_{\mathbf{n|n-1}})(\mathbf{y}_{\mathbf{n}} - \mathbf{y}_{\mathbf{n|n-1}})^T] \\ \mathbf{P}_{\mathbf{yy,n}} &= E[(\mathbf{y}_{\mathbf{n}} - \mathbf{y}_{\mathbf{n|n-1}})(\mathbf{y}_{\mathbf{n}} - \mathbf{y}_{\mathbf{n|n-1}})^T] \end{aligned} \tag{6.9}$$

When the state equation and measurement equation are not linear, the above equations of the covariances of the errors, $\mathbf{P_{n|n-1}}$ and $\mathbf{P_n}$, as well as the equation of the Kalman gain, $\mathbf{K_n}$, are not valid, and, therefore, generally, the Kalman gain cannot be analytically determined. A common approach to circumventing such problems in nonlinear state-space models is to apply EKF, which is a variant of the Kalman filter, that approximates the state and measurement equations by linearizing them using the Taylor series. Consequently, the EKF approximates the posterior probability density of the state vector by a Gaussian distribution. When the true posterior distribution of the state vector is not 'close' to Gaussian, such approximations may not be valid and the EKF may diverge. In such cases, sequential Monte Carlo methods show superior performance over EKF [86].

EnKF is the Monte Carlo-based Kalman filter that can be used for nonlinear and non-Gaussian models. The underlying idea of the method is to approximate the Kalman gain and state vector propagations using the Monte Carlo technique. EnKF computes the Kalman gain by approximating $\mathbf{P_{xy,n}}$ and $\mathbf{P_{yy,n}}$ using their corresponding sample covariances, $\hat{\mathbf{P}}_{\mathbf{xy,n}}$ and $\hat{\mathbf{P}}_{\mathbf{yy,n}}$. To do so, N number of ensembles, $\{\mathbf{x}_{n|n-1}^{(i)}\}_{i=1}^{N}$, are first drawn from the prior probability density of the state vector, $p(\mathbf{x}_{n|n-1})$, which has the same probability distribution function as the state noise with a mean of $f(\mathbf{x}_{n-1}^{(i)})$. Once the ensembles are generated, the sample covariances of the errors are computed as follows:

$$\begin{aligned}\hat{\mathbf{P}}_{\mathbf{xy,n}} &= \frac{1}{N}\sum_{i=1}^{N}(\mathbf{x}_{n|n-1}^{(i)} - \underline{\mathrm{x}}_n)(\mathbf{y}_{n|n-1}^{(i)} - \underline{\mathrm{y}}_n)^T \\ \hat{\mathbf{P}}_{\mathbf{yy,n}} &= \frac{1}{N}\sum_{i=1}^{N}(\mathbf{y}_{n|n-1}^{(i)} - \underline{\mathrm{y}}_n)(\mathbf{y}_{n|n-1}^{(i)} - \underline{\mathrm{y}}_n)^T\end{aligned} \tag{6.10}$$

where $\mathbf{y}_{\mathbf{n|n-1}}^{(\mathbf{i})} = h(\mathbf{x}_{n|n-1}^{(i)})$, $\underline{\mathrm{x}}_n = \frac{1}{N}\sum_{i=1}^{N}\mathbf{x}_{n|n-1}^{(i)}$

$$\underline{\mathrm{y}}_n = \frac{1}{N}\sum_{i=1}^{N}\mathbf{y}_{n|n-1}^{(i)} \tag{6.11}$$

Then, the Kalman gain is approximated by:

$$\hat{\mathbf{K}}_n = \hat{\mathbf{P}}_{\mathbf{xy,n}}(\hat{\mathbf{P}}_{\mathbf{yy,n}})^{-1} \tag{6.12}$$

and the ensembles of the state vector, $\{\mathbf{x}_{n|n-1}^{(i)}\}$, are computed as

$$\mathbf{x}_n^{(i)} = \mathbf{x}_{n|n-1}^{(i)} + \hat{\mathbf{K}}_n(\mathbf{y}_n + \mathbf{v}_n^{(i)} - \mathbf{y}_{n|n-1}^{(i)}) \tag{6.13}$$

where $\mathbf{v}_n^{(i)}$ are samples obtained from Gaussian distribution with mean $\mathbf{y}_n$ and covariance $\mathbf{Q_w}$. Once the ensembles of the state vector are computed, the estimate of the state vector is obtained by taking the averages of ensembles as follows:

$$\hat{\mathbf{x}}_n = \frac{1}{N}\sum_{i=1}^{N}(\mathbf{x}_n^{(i)}) \tag{6.14}$$

Figure 6.1 presents a complete basic operation of the EnKF.

6.3 EnKF based fECG Extraction Algorithm

6.3.1 State-Space Model of a Synthetic ECG

In the work reported in, McSharry et al. proposed a dynamic model which consists of a set of nonlinear state equations to generate synthetic ECG signals in the Cartesian coordinate system [85]. The model represents an ECG signal by a sum of five Gaussian functions, each corresponding to the five waves of an ECG signal, namely P, Q, R, S, and T waves. The state vector of the dynamic model is defined by $[x_k, y_k, z_k]^T$, and the state equation is given

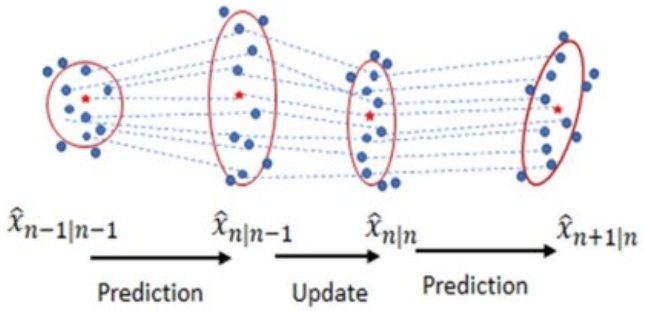

Initialize the state vector by estimating x_0

For i = 1 to N (*total number of ensembles*)

Draw N predicted ensembles

$$x^{(i)}{}_n \sim p\left(x_k \middle| x^{(i)}{}_{n-1}\right)$$

Compute the predicted values

$$y^{(i)}{}_{n|n-1} = [\,\emptyset_k, z^{(i)}{}_{k|k-1}]^T$$

$$x^{(i)}{}_{n|n-1} = F(x^{(i)}{}_{n-1|n-1})$$

$$\bar{x}_n = \frac{1}{N}\sum_{i=1}^{N} x^{(i)}{}_{n|n-1}, \bar{y}_n = \frac{1}{N}\sum_{i=1}^{N} y^{(i)}{}_{n|n-1}$$

Approximate the covariance of state error vectors

$$\hat{P}_{xy,n} = \frac{1}{N}\sum_{i=1}^{N}(x^{(i)}{}_{n|n-1} - \bar{x}_n)(y^{(i)}{}_{n|n-1} - \bar{y}_n)^T$$

$$\hat{P}_{yy,n} = \frac{1}{N}\sum_{i=1}^{N}(y^{(i)}{}_{n|n-1} - \bar{y}_n)(y^{(i)}{}_{n|n-1} - \bar{y}_n)^T$$

Compute the Kalman gain

$$\hat{K}_n = \hat{P}_{xy,n}\,(\hat{P}_{yy,n})^{-1}$$

Determine the ensemble of state vector

$$x^{(i)}{}_n = x^{(i)}{}_{n|n-1} + \hat{K}_n(y_n + v^{(i)}{}_n - y^{(i)}{}_{n|n-1})$$

Estimate the state vector

$$\hat{x}_n = \frac{1}{N}\sum_{i=1}^{N} x^{(i)}{}_n$$

Figure 6.1: An overview of EnKF. EnKF maintains an ensemble of sample points for the state vector x_n. It propagates and updates the ensemble to track the distribution of x_n. The state estimation is conducted by calculating the sample mean (red five-pointed-star) and covariance (red ellipse) of the ensemble.

by:

$$\begin{cases} x_k = \varphi x_{k-1} - \omega y_{k-1} \\ y_k = \varphi y_{k-1} + \omega x_{k-1} \\ z_k = -\sum_{i\in[P,Q,R,S,T]} \frac{a_i \Delta\theta_i w}{\beta_i^2} exp(-\frac{\Delta\theta_i^2}{2b_i^2}) - z_{k-1} \end{cases} \tag{6.15}$$

where x, y, and z are the state variables, $\varphi = 1 - \sqrt{x^2 + y^2}$, $\Delta\theta_i = (\theta - \theta_i) mod 2\pi$, $\theta = atan2(y, x)$ is the four quadrant arctangent of the elements of x and y, with $-\pi \leq atan2(y, x) \leq \pi$, and ω is the angular velocity of the trajectory as it moves around the limit cycle in the $x - y$ plane. The α_i, b_i, and θ_i represent the amplitude, width, and center of the Gaussian functions of the five PQRST waves, respectively. Further, Sameni et al. transformed the model to a polar coordinate system and provided a convenient discrete-time mathematical model [34]. The state vector of the dynamic model is defined by $[r_k, \theta_k, z_k]^T$, and the state equation is given by:

$$\begin{cases} r_k = r_{k-1}(1 - r_{k-1}) \\ \theta_k = \omega \\ z_k = -\sum_{i\in[P,Q,R,S,T]} \frac{a_i \Delta\theta_i w}{\beta_i^2} exp(-\frac{\Delta\theta_i^2}{2b_i^2}) - z_{k-1} \end{cases} \tag{6.16}$$

where r and θ are the radial and angular state variables in polar coordinates, respectively. The second and third equations of 6.16 are independent from radial. Therefore, this first equation may be excluded as it does not affect the synthetic ECG (the state variable). The simplified state vector of the dynamic model is defined by $\mathbf{x}_k = [\theta_k, z_k]^T$, and the state equation is given by:

$$\begin{cases} \theta_k = (\theta_{k-1} + \omega.\Delta) mod 2\pi \\ z_k = -\sum_{i\in[P,Q,R,S,T]} \frac{\alpha_i \Delta\theta_i \omega.\Delta}{b_i^2} exp(-\frac{\Delta\theta_i^2}{2b_i^2}) + z_{k-1} + \eta_k \end{cases} \tag{6.17}$$

where $\Delta\theta_i = (\theta_k - \theta_i) mod 2\pi$ is the phase increment, Δ is the sampling period, η_k is the state noise, ω is the angular velocity of the trajectory as it moves around the limit cycle, and α_i, b_i, and θ_i represent the amplitude, width, and center of the Gaussian functions of the five PQRST waves, respectively.

The measurement vector is defined by $\mathbf{y}_k = [\phi_k, s_k]^T$, where ϕ_k is the observed phase representing the linear time wrapping of the R-R time interval into $[0, 2\pi]$, and s_k is the observed amplitude. The measurement equation is given by

$$\begin{cases} \phi_k = \theta_k + u_k \\ s_k = Z_k + v_k \end{cases} \tag{6.18}$$

where u_k and v_k denote the measurement noises.

6.3.2 Fetal QRS Detection with EnKF

Given the state-space model 6.17 and 6.18, the EnKF algorithm is applied to filter out the mECG from aECG, assuming the remaining signal composed of fECG and noise is Gaussian distributed. The extracted mECG signal is then subtracted from aECG to obtain a noisy fECG signal. Finally, the EnKF algorithm is applied to the residual signal to denoise the fECG signal, as shown in Figure 6.2.

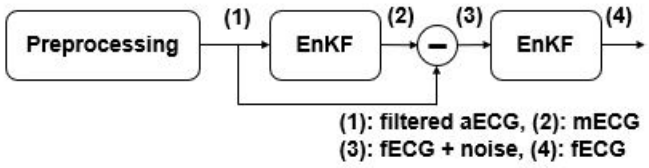

Figure 6.2: Fetal QRS (fQRS) detection process: (1) Preprocessing step ; (2) Ensembel Kalman filter (EnKF) applied for maternal ECG (mECG) extraction; (3) mECG subtracted from filtered aECG signal and EKF used for fetal ECG (fECG) extraction; (4) EnKF applied for fECG extraction.

6.3.3 Preprocessing

A wide range of noise sources affect a recorded aECG signal. External electrical interferences generate high-frequency noise and other sources, such as muscular activity or breathing, produce low-frequency noise, which causes baseline drift [87, 88, 89, 90]. The low-frequency noise is more pronounced when the subject is exercising. The frequency range of the baseline wander is usually less than $1Hz$ [91, 88]. We remove the aECG baseline wander by filtering the aECG signal using a second-order low-pass filter with a cut-off frequency of $1Hz$. The output of the low-pass filter is the estimate of the baseline wander, which is subtracted from the ECG signal to obtain the pre-processed aECG signal [92, 88],

$$pre - processed\_aECG = aECG - baseline \tag{6.19}$$

A notch filter is also used to suppress the powerline interference noise. We also applied the wavelet filtering (a 10 level 1-D stationary wavelet decomposition with Coiflet mother wavelet) and thresholding technique. This will be discussed in detail in section 6.5. Finally, the fetal QRS complex (fQRS) is detected using the Pan-Tompkin algorithm [13, 88].

6.4 Results

The execution time of each algorithm is calculated from the start of the pre-processing to the end of the fECG R-peak detection. The EnKF with an ensemble size of 70 has the same execution time as the EKF. Hence, the proposed EnKF-based algorithm was run with an ensemble size of N = 70 for single-channel signals from the aforementioned datasets. For comparison purposes, the EKF-based algorithm using the same synthetic ECG parameters and datasets was also carried out. The three-dimensional trajectory generated from equation 6.17 consists of a unit-radius circular limit cycle that goes up and down when it approaches

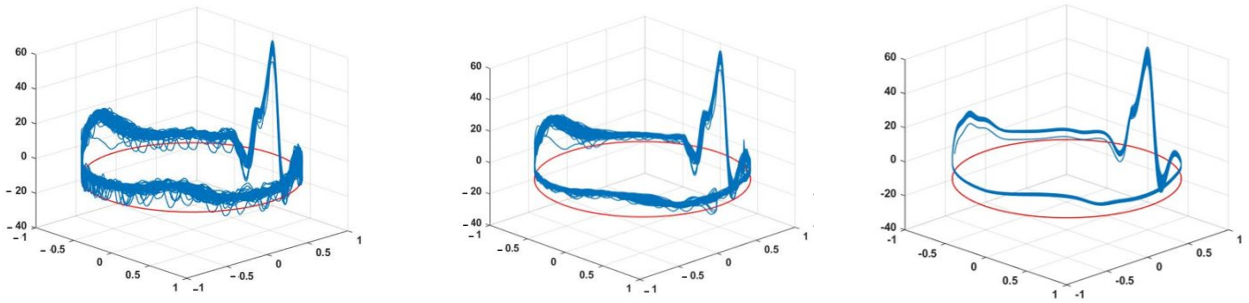

(a) (b) (c)

Figure 6.3: A phase-wrapped ECG signal of records "a01". (a) Abdominal ECG (raw data); (b) mECG extracted using EKF; and (c) mECG extracted using our EnKF.

one of the P, Q, R, S, or T points (Figure 6.3). The projection of these trajectory points on the z-axis gives a synthetic ECG signal. Figure 6.3 shows plots of the ECG signals versus the assigned phases in polar coordinates on the unit-radius circle. The figure depicts a typical phase-wrapped aECG signal (a), EKF extracted mECG signal (b), and EnKF extracted mECG signal (c) plotted using a sample signal taken from the PhysioNet database.

Examples of two abdominal ECG signals of records "a01", and "a03", and fetal signals extracted using the EKF and EnKF, are shown in Figure 6.4. Panels 6.4a, 6.4d and 6.4g are the original signals. Panels 6.4b, 6.4e and 6.4h are fQRS extracted using the EKF, while 6.4c, 6.4f and 6.4i are fQRS extracted using the EnKF approaches, respectively. The fQRS annotation is shown in an orange asterisk (*). The red arrows show the places where fetal QRS was wrongly detected. The blue arrows show the missing fetal QRS. It can be seen that the detected fQRS (fetal R-peaks) follow the an-notated ones with high accuracy. It is worth noting that in "a01" (6.4d), the fetal QRS complexes are reversed due to electrode placement, but it did not affect the extraction algorithms. It should be emphasized that in the case of overlapping of the fetal QRS and maternal QRS, the EnKF algorithm still gives favorable results. Comparison between Figure 6.4b,and 6.4c show that the EKF failed when maternal and fetal QRS complexes overlap in time (e.g., at t $= 21.8$ s and t $= 23.7$ s) for 'a03', while our EnKF method still performed successfully. It can be also seen that the EnKF functions reasonably well in the presence of noise (e.g., at t $= 19.7$ s for 'a01', Figure

6.4d - 6.4f).

Figure 6.5 depicts the fECG extraction results from the modified PhysioNet data with added motion artifacts. As seen, the fECG extracted by the EKF was incorrect and its F1 score was reduced significantly (average F1=78, see Table 6.1). fQRS complexes extracted by the EnKF, however, are still visible in most time points, yielding a favorable F1 score of 89.

Figure 6.6 shows the performance of the proposed algorithm, the EnKF, and the EKF on one sample from our clinical data. Panels 6.6a - 6.6c show original and extracted signals, while panels 6.6d - 6.6f are signals with extensive preprocessing. Specifically, in Figure 6.6d, a lowpass filter (with a cut-off frequency of 1 Hz), a notch filter, and a Wavelet filter (a 10 level 1-D stationary wavelet decomposition with Coiflet mother wavelet) were used to suppress the background noise and artifacts. The signal extracted from the preprocessed data with the EKF and EnKF algorithms are shown in Figure 6.6e and 6.6f. In Figure 6.6f, we also further notice that fetal characteristic waves, such as P and T waves, may be conserved. This judgment is also strengthened by the EnKF extraction carried out on the original PhysioNet database in Figure 6.4f, where the conserved features are probably fECG waves. Table 6.1 presents the average F1, average PPV, and average SE results in our own clinical aECG records. The average F1, PPV, and SE indices of our proposed EnKF are 94.3%, 100%, and 89.2%; while those using the EKF method are 82.3%, 71.4%, and 100%, respectively.

Table 6.1 shows the average F1 scores, the average PPE, and the average SE of the performance of the EnKF and EKF algorithms. These statistical indices are computed by determining the accuracy, TP, FP, and FN, of the locations of the R-peaks obtained by the EKF and EnKF algorithms against the reference annotations. The F1 score, PPV, and SE are computed using 68 one-minute aECG records from PhysioNet 2013 Challenge databank and our own clinical data. The results shown in Table 6.1 indicate that the EnKF method is reliable on its own. In all cases, the EnKF outperforms the EKF. Another parameter that

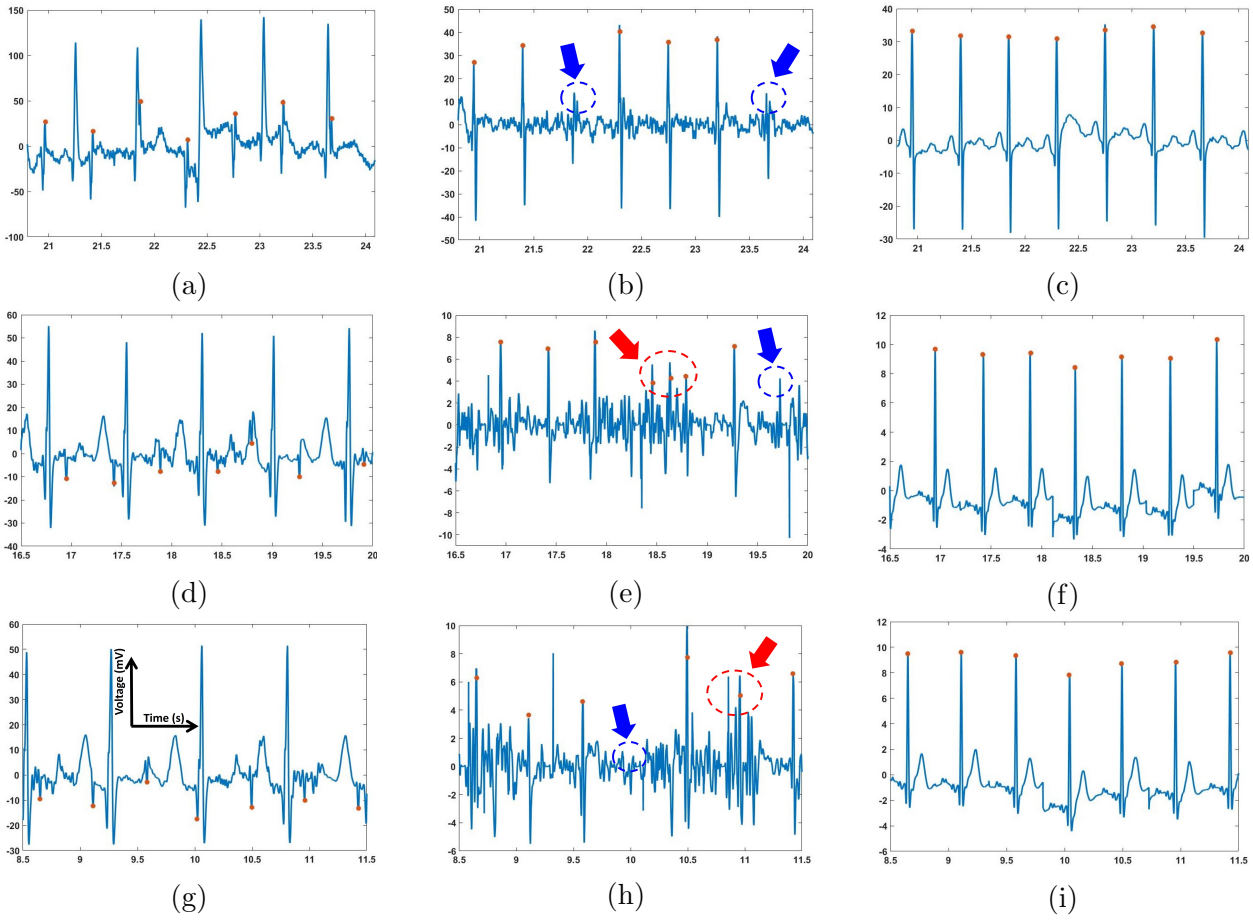

Figure 6.4: fECG extraction using the EKF and EnKF with the PhysioNet data. The fQRS annotation is shown in orange asterisk (*). The red arrows show the places that fetal QRS was wrongly detected. The blue arrows show the missing fetal QRS. (a) Abdominal ECG (raw data) of record "a03"; (b) fECG extracted using EKF of record "a03"; (c) fECG extracted using EnKF of record "a03"; (d) Abdominal ECG (raw data) of record "a01" with reversed fetal QRS complexes; (e) fECG extracted using EKF of record "a01"; (f) fECG extracted using EnKF of record "a01". (g) Abdominal ECG (raw data) of record "a01" with reversed fetal QRS complexes; (h) fECG extracted using EKF of record "a01"; (i) fECG extracted using EnKF of record "a01".

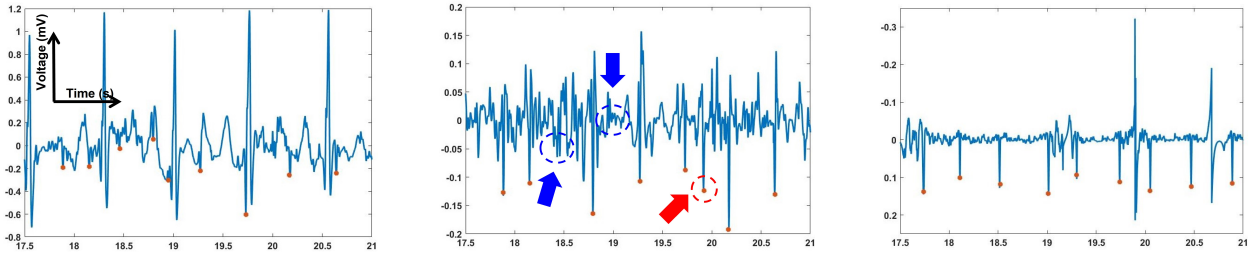

(a) (b) (c)

Figure 6.5: fECG extraction using the EKF and EnKF with the motion artifacts added PhysioNet data. The fQRS annotation is shown in orange asterisk (*). The red arrows show the places that fetal QRS was wrongly detected. The blue arrows show the missing fetal QRS. (a) Abdominal ECG (raw data); (b) fECG extracted using EKF; and (c) fECG extracted using EnKF.

should be taken into account is computational complexity. The computational complexity of the EnKF algorithm is proportional to the number of ensembles used. In our simulations, we have observed that increasing the size of the ensemble by more than 70 does not improve the performance of the algorithm significantly. The F1 score obtained when the algorithm was run for ensemble sizes between 5 to 350 always remained in the range between 94.5% and 98.6% for all the 68 aECG records obtained from the PhysioNet database.

Table 6.1: Performance of the EKF and EnKF algorithms.

Data	Method	F1 (%)	SE (%)	PPE (%)
Online Data without Motion Noise	EKF	88.90 ± 5	86.73 ± 5.5	91.16 ± 4.6
	EnKF	97.25 ± 2.4	96.91 ± 0.5	97.59 ± 3.8
Online Data with Motion Noise	EKF	78 ± 6.58	75.38 ± 7.4	80.80 ± 5.1
	EnKF	89.04 ± 3	88.2 ± 1.7	89.9 ± 4.5
Our Clinical Data	EKF	82.3 ± 5.5	100 ± 0.1	71.4 ± 6.4
	EnKF	94.3 ± 1.2	89.2 ± 1.5	100 ± 0.2

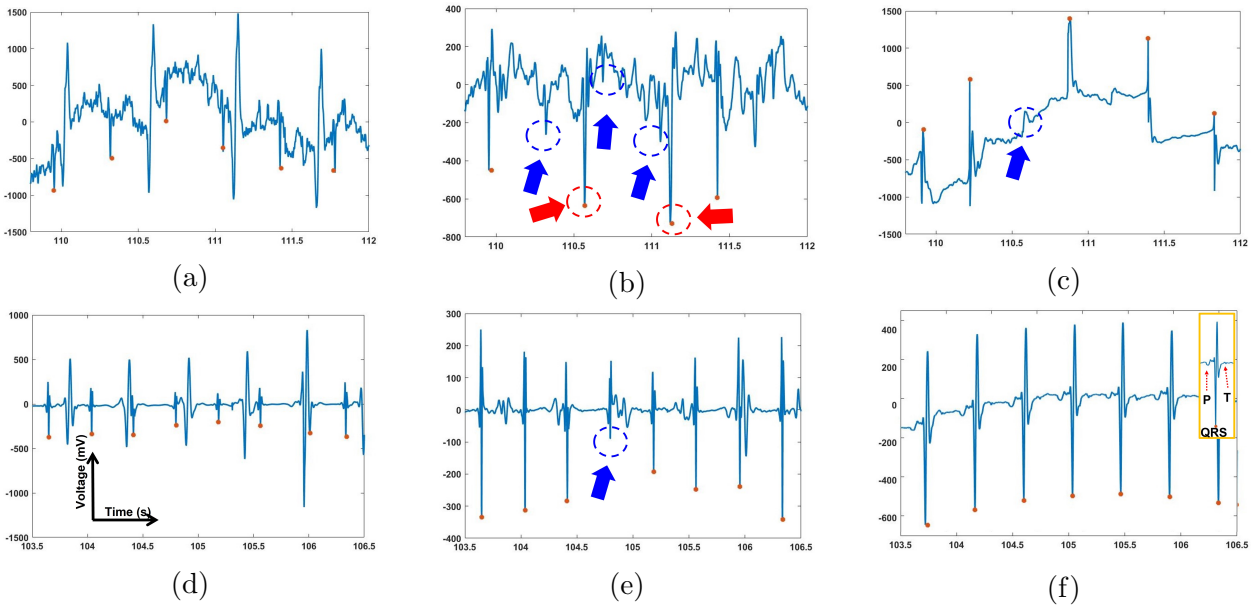

Figure 6.6: fECG extraction using the EKF and EnKF with our own clinical data. The fQRS annotation is shown in orange asterisk (*). The red arrows show the places that fetal QRS was wrongly detected. The blue arrows show the missing fetal QRS. (a) Abdominal ECG (raw data), (b) fECG extracted from EKF and (c) fECG extracted from EnKF". (d) Abdominal ECG after Wavelet preprocessing; (e) fECG extracted using EKF of preprocessed data; and (f) fECG extracted using EnKF of preprocessed data. The inset shows additional peaks, likely P and T waves; they were conserved after EnKF extraction.

6.5 Discussion

The current fECG extraction methods from a single-channel signal are not robust when particularly i) the fECG and mECG waveforms temporally overlap, and ii) the amplitude of fECG is low compared to the noise level. Recently, an EKF-based algorithm was proposed for the extraction fECG from a single-channel aECG signal [43]. Generally, those EKF-based algorithms are less effective as at every instant of time, they approximate the posterior probability density of the parameter of interest by a Gaussian distribution. When the true posterior density is not Gaussian, Sequential Monte Carlo (SMC) filtering methods show superior performance over EKF methods. Therefore, here, our proposed EnKF is an SMC-based method, for noninvasive extraction of fECG from the single-channel aECG. As described above, our EnKF-based algorithm exhibited robust performance when tested using

public online data as well as our own clinical data. Ten records, including 20-min aECG from our own clinical database, 68 records, including 1-min aECGs in PhysioNet Challenge 2013, and the online data bank added realistic motion artifacts were used to assess the performance of the proposed method.

As can be seen in Figure 6.3, the EnKF-based algorithm follows the dynamics of ECG and thus suppresses the noise better than EKF. In the EKF method, since some of the fECG peaks were still incorporated in the estimated mECG (6.3b), the subtraction between the aECG and mECG will not produce the correct fECG. In contrast, the mECG estimated by EnKF is significantly clearer (6.3c), which explains the better performance in fECG extraction (Figure 6.4, Figure 6.5, Figure 6.6 and Table 6.1). Our experiments proved that the EnKF-based algorithm is a robust method and has superior performance over the EKF for extracting fECG in various scenarios (Figure 6.4, Figure 6.5, and Figure 6.6). Results support the expectations that the EnKF not only extracts the fetal signal when the fECG and mECG waveforms temporally over-lap, but it also potentially extracts accurate fECG signal with characteristic waves such as P and T waves. Currently, there is no approach available to extract full-feature fECG, especially with aECG in daily life. Hence, our solution may hold the potential to revolutionize fetal monitoring as it can be used to diagnose potential congenital effects. Currently, this is carried out with genetic test and echocardiogram [93, 94, 95]. However, those need to be done in the clinics and they cannot provide continuous information of the fetal heart over a long period of time. For example, with our fetal ECG patch and this EnKF method, full-feature fECG can be obtained 24/7 in the home setting in the second and third trimesters of pregnancy, which provides information about not only fetal wellbeing and development but also any fetal cardiac anomalies.

Due to the nature of aECG acquisition, the signal is always accompanied by other bioelectric potentials, such as maternal muscle activity, fetal movement activity, and noise [33]. The results are shown in Figure 6.4, Figure 6.5, and Figure 6.6 suggested that, prior to fECG

extraction, preprocessing is a critical step that needs to be optimized. Specifically, preprocessing may help extraction significantly as it removes noise components, but it may also eliminate low-amplitude precious components such as P and T waves. In Figure 6.6d, we can see that, when the aECG signal is somewhat over-processed, both EKF and EnKF perform reasonably well; the signal, however, may have lost its intrinsic peaks. The filtering scheme used here is a low-pass filter, a digital Notch filter, and the wavelet filtering and thresholding technique described in [76]. As P and T waves have similar frequency and amplitude to noise components, it is almost impossible to set up optimal thresholds to eliminate the noise and keep the desired waves in all cases. Therefore, we usually carry out this manually until the best performance is obtained.

Chapter 7

ECG Denoising Using the EnKF

7.1 Introduction

In this chapter, we propose and develop a novel algorithm based on the Ensemble Kalman Filter (EnKF) to remove noise in ECG signals.

7.2 Review of ECG denoising methods

Several methods have been proposed to filter ECG from the signal contaminated with undesired interferences; however, each has its advantages and limitations. These methods include using smoothing filters such as Savitzky-Golay filtering (SG) [96], Extended Kalman Filter (EKF) [97], Wavelet Denoising (WD) [96], Empirical Mode Decomposition (EMD) [98], Ensemble Empirical Mode Decomposition (EEMD) [99], adaptive filtering like Recursive Least Squares Filter (RLS) and Normalized Least-Mean-Square Filter (NLMS) [96], Total Variation Denoising (TVD) [100], Sparsity [101], among others. One study on ECG signals with noise levels from 5 dB signal to noise ratio (SNR) to 45 dB SNR showed that the

WD performs better denoising than the others. However, SG and the Adaptive filter like RLS and NLMS perform better in some mid-range SNR [96]. The EKF is also a promising tool for ECG denoising; however, the filter model is highly reliant on the underlying dynamics assumed for the ECG signal and not practical for nonlinear models in a realistic environment [97]. Zebin et al. reported that after decomposing the ECG signal using EMD and applying soft wavelet thresholding to the high-frequency components, the reconstructed signal was denoised more effectively than if only one method were applied [98]. Kumar et al. applied TVD successfully for detecting R-peak signals with long-pause, drifts, complexes QRS, smaller R peaks, and even noisy signal portions. However, TVD is still comparatively less accurate than other methods for detecting false-positive and false-negative [100].

7.3 Methods

The Kalman Filter (KF) was initiated by R. E. Kalman for linear models and the noises involved are additive [78]. For nonlinear cases, EKF has been widely used, which is based on local linearization of the nonlinear model using the Jacobian [79]. The EKF-based algorithms have a drawback in that, at every instant of time, they approximate the posterior probability density of the parameter of interest by a Gaussian distribution. When the true posterior density is not Gaussian, Sequential Monte Carlo (SMC) filtering methods show superior performance over EKF methods. G. Evensen introduced the EnKF which is an approximate filtering method that represents the distribution of the state with an ensemble of draws from that distribution [80]. The EnKF is described in detail in Chapter 6. The EnKF is illustrated in Figure 7.1.

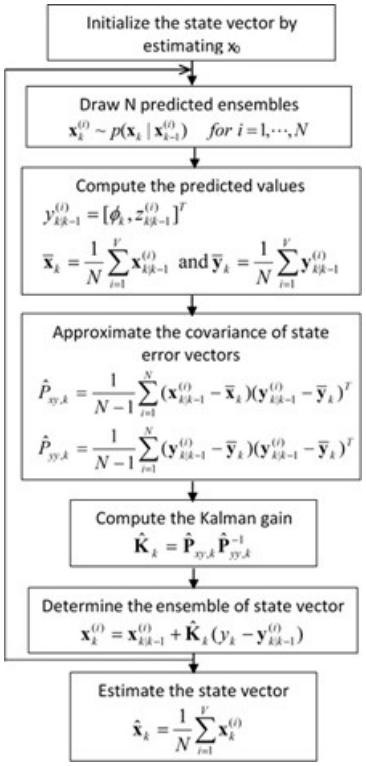

Figure 7.1: The EnKF algorithm flow chart.

7.4 Results

The three-dimensional trajectory which is generated from (8), consists of a unit circular (r=1) limit cycle which is going up and down when it approaches one of the P, Q, R, S, or T points. The projection of these trajectory points on the z-axis gives a synthetic ECG signal. We intensively explored various filtering algorithms, including EKF, SG, WD, EEMD, LMS, RLS, and TVD. Figure 7.2 illustrates the typical phase-wrapped results of the EnKF, EKF, SG, WD, EEMD, LMS, RLS, and the TVD for an input SNR of 12 dB.

The performance in ECG denoising for all the methods are evaluated and qualitatively compared in Figure 7.3. This figure presents the enhanced ECG signals in the time domain obtained by using the methods mentioned above.

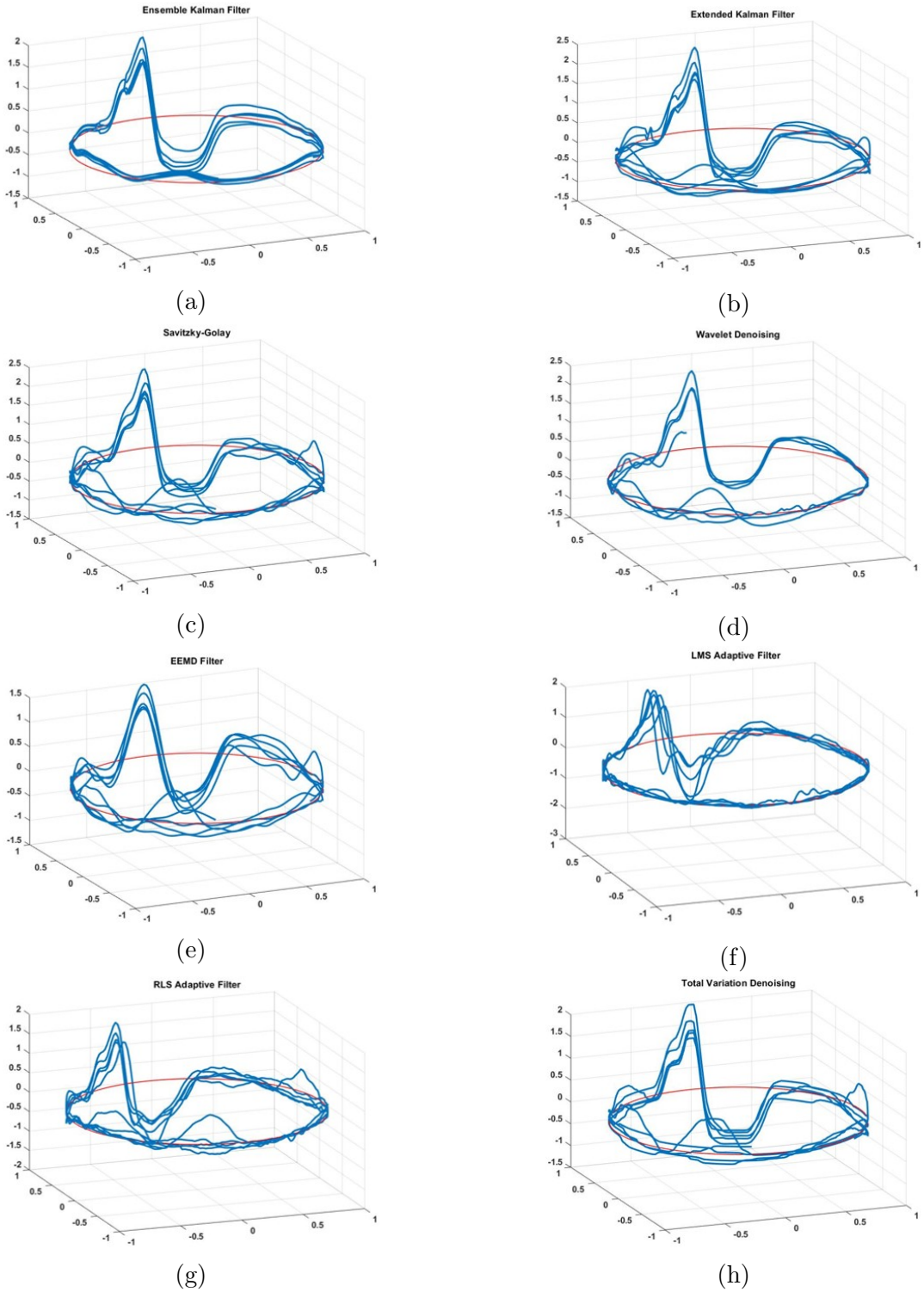

Figure 7.2: phase-wrapped ECG filtering results for an input signal of 12 dB. (a) EnKF. (b)EKF. (c) SG. (d) Wavelete. (e) EEMD Filter. (f) LMS Adaptive Filter. (g) RLS Adaptive Filter. (h) Total Variation Denoising.

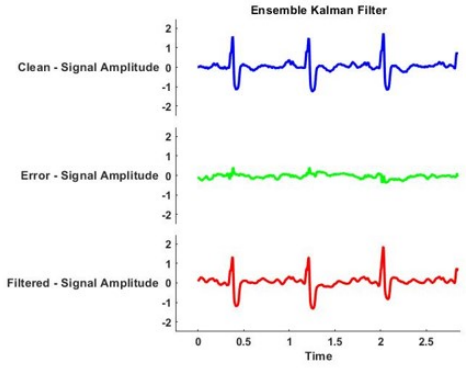
Ensemble Kalman Filter
Clean - Signal Amplitude
Error - Signal Amplitude
Filtered - Signal Amplitude
Time

(a)

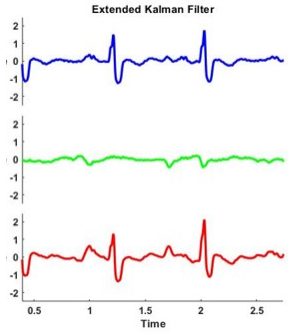
Extended Kalman Filter
Time

(b)

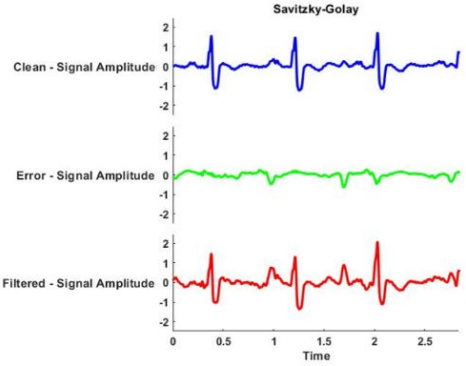
Savitzky-Golay
Clean - Signal Amplitude
Error - Signal Amplitude
Filtered - Signal Amplitude
Time

(c)

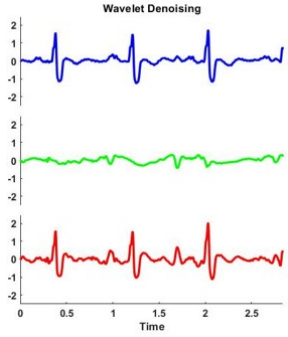
Wavelet Denoising
Time

(d)

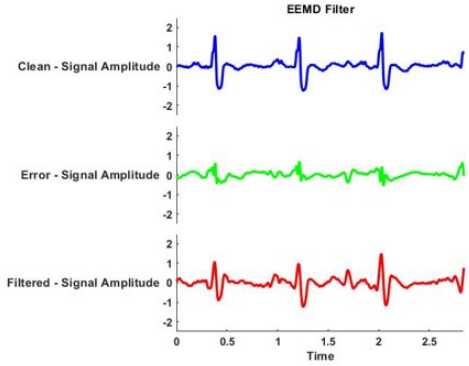
EEMD Filter
Clean - Signal Amplitude
Error - Signal Amplitude
Filtered - Signal Amplitude
Time

(e)

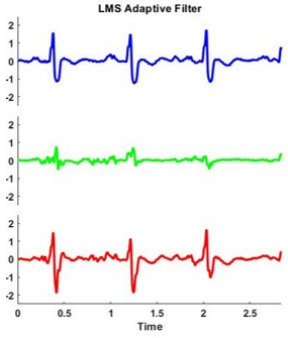
LMS Adaptive Filter
Time

(f)

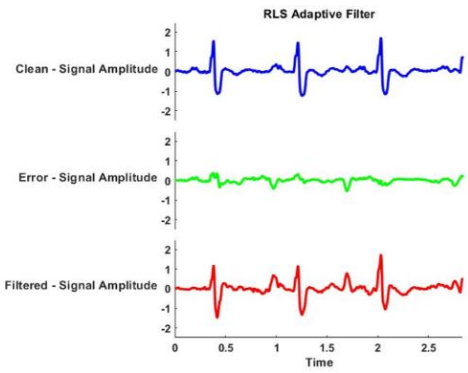

(g)

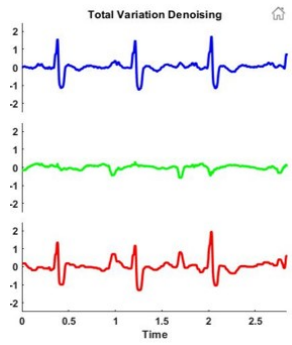

(h)

Figure 7.3: Enhanced ECG signals in time domain obtained by using different denoising methods. (a) EnKF. (b)EKF. (c) SG. (d) Wavelete. (e) EEMD Filter. (f) LMS Adaptive Filter. (g) RLS Adaptive Filter. (h) Total Variation Denoising.

The signal under test is the record 118 from the MIT-BIH Arrhythmia Database with different SNR from 6 to 24 dB. The efficacy of the denoising techniques with the different input SNR levels is described in Figure 7.4. The records from the MIT-BIH database are used. For each record, the SNR is changed from 6 to 18 dB. This figure presents the SNR improvement, PRD, Correlation, and RMSE for all the denoising techniques, at different levels of noise. Table 7.1 presents the performance of all filtering algorithms at the modified MIT-BIH database with added motion artifacts.

7.5 Discussion

The denoising problem is approached by a new technique, the EnKF. This approach has overcome denoising ECG signals in low input SNRs and in non-Gaussian and non-stationary situations. In Figure 7.2, results for filtering ECG performed by EnKF, EKF, SG, WD, EEMD, LMS, RLS, and TVD are depicted. As seen, the EnKF has followed the dynamics of the ECG signal and it has suppressed the noise more than the other methods. The proposed method, EnKF, is compared with the widely used filtering methods and demonstrates better results in terms of visual quality. TVD and LMS annihilate the morphology of ECG

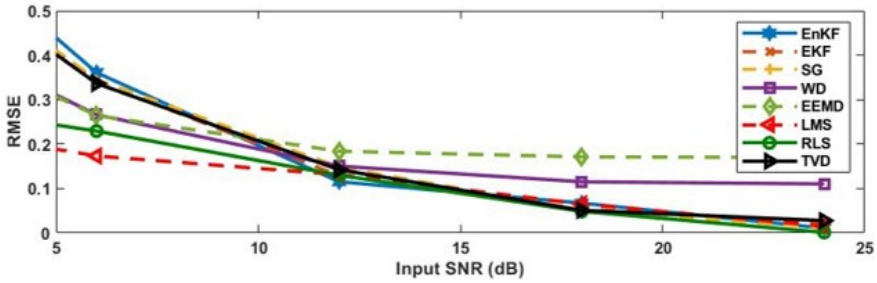

(a)

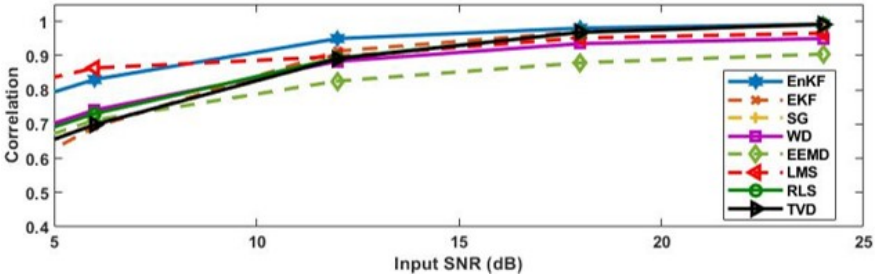

(b)

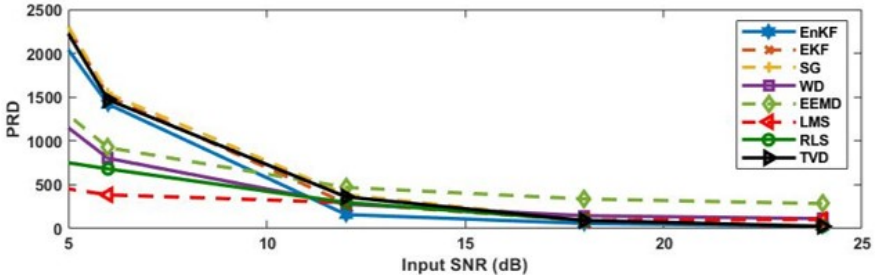

(c)

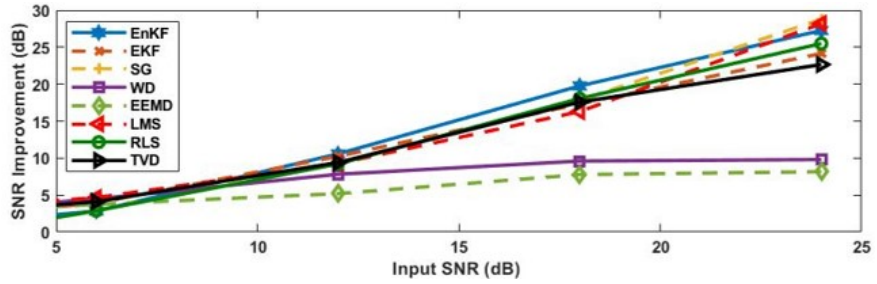

(d)

Figure 7.4: (a) Comparison of the mean RMSE obtained by using different denoising methods at different input SNR levels. (b) Comparison of the mean Correlation versus different input SNR levels. (c) Comparison of the PRD for different denoising methods at different input SNR levels. (d) Comparison of the mean SNR improvements for different denoising methods versus different input SNR levels.

Table 7.1: Performance of denoising of algorithms for the motion noise cancellation.

	SNR	**Correlation**	**PRD**	**RMSE**
EnKF	10.965	0.959	150.45	0.105
EKF	10.226	0.913	288.18	0.128
SG	9.280	0.888	387.12	0.148
WD	7.813	0.883	277.82	0.150
EEMD	5.187	0.825	469.50	0.183
LMS	9.254	0.897	297.12	0.131
RLS	9.206	0.892	298.15	0.129
TVD	9.397	0.890	361.32	0.142

which contains useful information. The SG, EEMD, and RLS could not eliminate the noise completely. The results of WD, and EKF are fairly consistent.

Figure 7.3 reveals that the denoised signals are more distorted in the case of the other methods. It is to be mentioned that the pattern of the enhanced ECG signal resulting from the proposed method resembles the original ECG signal more and seems smoother in comparison to the signal obtained from the other methods.

Figure 7.4 illustrates the performance of different denoising methods at different input SNR levels. This figure compares RMSE, Correlation, PRD, and SNR of different denoising methods. Figure 7.4a presents the comparison of the RMSE results obtained by using different denoising methods at the various level of SNR. As seen, for particular SNR levels, the proposed method yields the smallest RMSE thus demonstrating its capability to yield enhanced ECG signal with better quality. Figure 7.4b depicts the correlation results for different input SNR levels. The proposed method has the maximum correlation with the clean signal.

The proposed method provided a significantly higher Correlation when compared with the other existing techniques. Figure 7.4c indicates that the proposed denoising method provides lower PRD than the other methods considered. The mean of the SNR improvements versus different input SNRs is plotted in Figure 7.4d. It is worth noting that EnKF has better performance in input SNRs greater than 10 dB. Visually comparing these results, it can be found the proposed methods have admirably tracked the original signal. This figure shows that the proposed method provided reasonably higher SNR in the higher SNR input level. To show that EnKF improvement is effective in daily life situations, the method has been validated using the modified data with motion noise added.

Table 7.1 shows the denoising performance comparison in terms of RMSE. Correlation, PRD, and SNR at the modified MIT-BIH database with added motion artifacts. It can be seen from the table that the EnKF has the highest SNR improvement. The same conclusion can be drawn from the PRD, Correlation.

The effectiveness of the EnKF in ECG denoising is shown through different databases. The proposed technique can be applied in the home ECG monitoring devices.

Chapter 8

Comparison of Methods to Extract Fetal Electrocardiogram

8.1 Introduction

The focus of this chapter is, first, to perform and compare different extraction algorithms and, second, to simulate practical noises to examine the algorithms in real situations. Data from the PhysioNet 2013 Challenge with labeled QRS complex annotations were used in the original form and with Gaussian and motion noise added, mimicking a practical scenario (See 4.2.1, 4.2.4). Our results in terms of accuracy, execution time, and robustness could provide useful insights into the implementation and operation of state-of-the-art fetal and maternal monitoring systems in the era of m-Health.

8.2 Methods

The methods for fetal electrocardiogram (fECG) extraction can be classified into three groups: blind source separation (BSS), template subtraction, and filtering techniques. The BSS methods assume that the abdominal signal is a mixture of independent signals, consisting of fECG, maternal electrocardiogram (mECG), and noises [26]. The template subtraction method may result in erroneous outcomes when the fECG and mECG waveforms temporally overlap. Our group has developed a novel f/mECG monitoring system, with which data would be collected from the abdomen [65]. The first system utilized the least-mean square adaptive filtering. Since the filtering requires the convergence of the adaptive filter, the stability depends on the choice of the step size. Our group also has used the BSS method under the independent component analysis (ICA) framework to extract fECG [46].

In this work, we explored JADE, FastICA and RobustICA, EKF, and TS algorithms for fECG extraction to evaluate their efficacy in terms of accuracy, computational complexity, and noise robustness (See 3). Furthermore, we attempted to use the combinations as (1) TS-ICA in which the abdominal electrocardiograms (aECGs) were first applied TS method to remove the mECG component, ICA method was then used to extract fECG. This method is useful as mECG's amplitude is dominant in the aECG, the use of TS may help to retain the fECG component; (2) ICA-TS in which the aECGs were first applied by ICA method, and four new separated signals produced were then put through the TS method. Utilizing ICA at the beginning is for extracting fECG, mECG, and other components; however, it does not completely remove mECG in the extracted fECG. Thus, applying the TS method could eliminate the remaining mECG component; and (3) ICA–TS–ICA in which the aECGs went through three steps; specifically, after removing mECG from the residual of (ICA-TS), ICA could be used again. It may have better results because four sources in residual signals have not shown mECG, so with using ICA in the last step, there will be three noise channels and one fECG channel.

8.3 Results

Figure 8.1 presents the performance of fQRS detection by TS (See 3.5). The aECG signals were preprocessed to remove the baseline wander, power line noise, and high-frequency noise. Then, the Pan-Tompkin algorithm was implemented on four aECG signals, resulting in R peaks of mECG (mQRS detection), as shown in Figure 8.1a. After mQRS detection, a template mECG was produced (Figure 8.1b). The following step is removing the template mECG signal by subtracting it out from the aECG signal. Finally, fetal QRS complex (fQRS) was detected using the Pan-Tompkin algorithm, as shown in Figure 8.1c. Table 8.1 represents

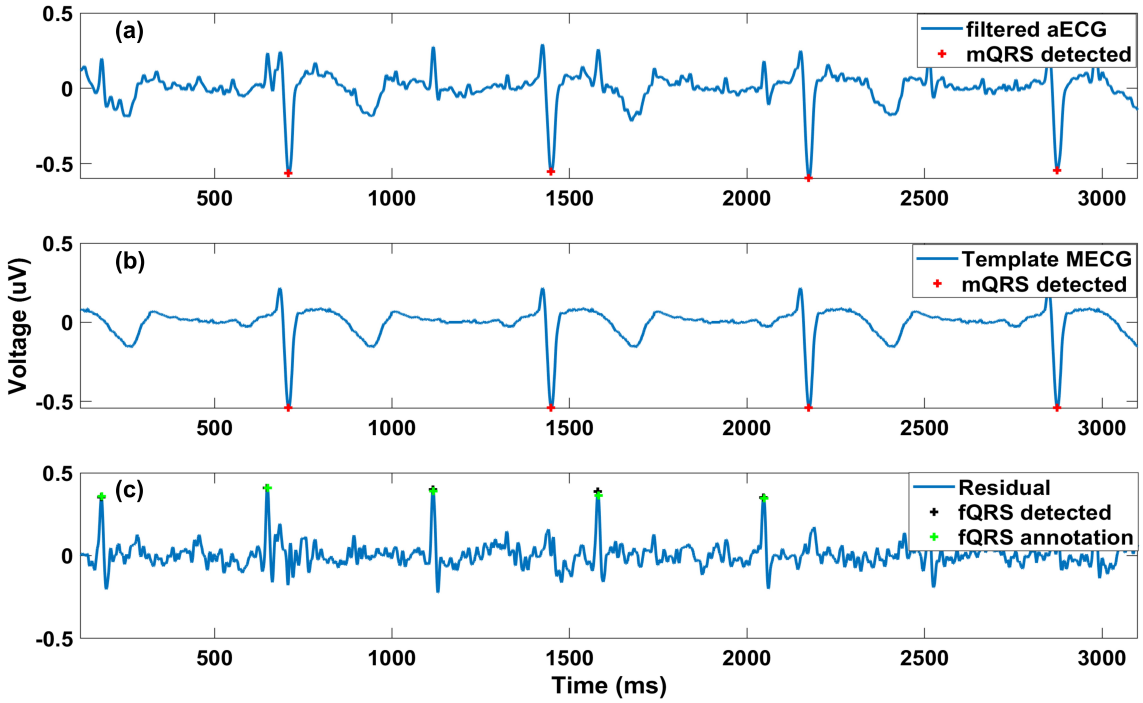

Figure 8.1: fQRS detection illustrated by TS method: (a) the aECG signal is filtered baseline wander and power line and applied Pan-Tompkins for mQRS detection; (b) a template of mECG is constructed from filtered aECG and the R peaks of mECG; (c): the residual signal is derived by the subtraction between filtered aECG and template mECG and Pan-Tompkins is applied for fQRS detection. The fQRS annotation is also included (plus sign in green).

the results of the average F1 score in the 68 aECG records using different approaches. The combination of TS-FastICA yielded the highest F1 score with 92.61%, followed by JADE-

TS-JADE and TS-JADE methods with 91.56% and 91. 16%, respectively. The lowest F1 scores were found in EKF, JADE, FastICA, and RobustICA with 54.34%, 61.27%, 60.08%, and 59.60%, respectively. It should be noted that using these algorithms alone was not as effective as that combined with other algorithms. Once motion noise was added, the F1 score was reduced significantly. More specifically, the highest F1 score was below 90%, including TS-RobustICA, JADE-TS, and JADE-TS-JADE. The lowest F1 was from EKF with 51.45%.

In Table 8.2, the number of records that had an F1 score lower than 50% is illustrated, providing a comprehensive assessment of the reliability of each approach. Specifically, the use of a combination of different approaches resulted in the lowest records with an F1 score below 50% while using an individual approach increased the number of records with an F1 score below 50%, especially in EKF with 38 out of 68 records. Similarly, the data with added motion noise showed a higher number of recordings with an F1 score below 50% which is reasonable as motion noise may dominate fECG which has lower amplitudes.

The performance of studied approaches with noise-added data is described in Figure 8.2. It is obvious that with higher noise levels, lower F1 was achieved. All approaches showed a linear curve for the F1 score when increasing the noise level, except for EKF. The F1 score in EKF slightly increased in noise level 3, compared with that in noise level 0. It could be explained that the noise added may superimpose the fECG signal, easing inadvertently this method to find peaks of fECG signal.

Memory requirement is not very important when algorithms are implemented on nowadays' computers; however, it will be important when mobile platforms with limited computation power are used, especially in real-time. For this calculation, the memory function in Matlab is used. Results are dependent on the computer hardware and the load on the computer. Table 8.3 shows the amount of memory used for each algorithm. The EKF method occupied the highest memory capacity with 2940 MB while other algorithms showed memory occu-

Table 8.1: Average F1 score(%) with different methods.

Method	Without motion noise	With motion noise
EKF	54.34	51.45
JADE	61.27	59.81
FastICA	60.08	59.38
RobustICA	59.60	58.74
TS	82.65	71.02
TSc	83.12	70.64
TS-JADE	91.16	82.35
TS-FastICA	92.61	85.02
TS-RobustICA	90.71	80.63
JADE-TS	90.57	85.10
FastICA-TS	82.98	77.94
RobustICA-TS	87.43	83.21
JADE-TS-JADE	91.56	85.43
FastICA-TS-FastICA	87.07	82.47
RobustICA-TS-RobustICA	89.29	82.67

Table 8.2: Number of records out of 68 datasets with F1 scores less than 50%.

Method	Without motion noise	With motion noise
EKF	38	40
JADE	18	19
FastICA	22	27
RobustICA	28	28
TS	10	17
TSc	10	17
TS-JADE	1	7
TS-FastICA	1	4
TS-RobustICA	2	8
JADE-TS	0	3
FastICA-TS	6	9
RobustICA-TS	5	5
JADE-TS-JADE	1	1
FastICA-TS-FastICA	5	5
RobustICA-TS-RobustICA	2	5

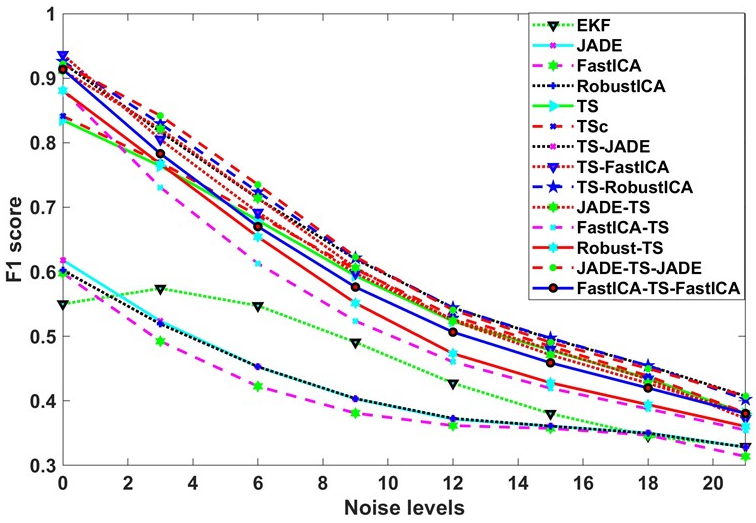

Figure 8.2: F1 comparison with different Gaussian noise levels.

pied below 1300 MB. Although the combination of different methods could provide higher performance i.e., higher a F1 score, it took a higher amount of memory than running them individually. For both high performance and low memory occupied cases, JADE-TS-JADE would satisfy those criteria.

This assessment aims to compare the complexity among methods, hereby providing suggestions to implement the algorithms on other platforms with different computational capacities. Here, a computer with the following configuration was used: Intel Core i5-8400 CPU @ 2.80GHz 6 Cores; Window 10 Education x64bit; RAM 16GB DDR4, and the software Matlab R2016. The execution time of each algorithm is calculated from the end of pre-processing to the end of R peak detection. Figure 8.3 depicts the time execution ran multiple times for each algorithm. In general, the time execution did not change significantly during each run. The approaches with the FastICA method including e.g., FastICA-TS-FastICA, TS-FastICA, FastICA-TS, FastICA, etc. showed the highest time execution with nearly 1 s. Other approaches fluctuated within 0.75 s in the first few running and stayed at 0.3 s after that. TS and TSc methods took the lowest time for finishing the program.

In EKF, we used a beat fitter module that calculates α_i and b_i (α_i and b_i represent the

Table 8.3: Required memory for different methods.

Method	Required Memory (MB)
EKF	2940
JADE	1175
FastICA	1183
RobustICA	1199
TS	1220
TSc	1205
TS-JADE	1204
TS-FastICA	1211
TS-RobustICA	1210
JADE-TS	1222
FastICA-TS	1206
RobustICA-TS	1199
JADE-TS-JADE	1192
FastICA-TS-FastICA	1199
RobustICA-TS-RobustICA	1202

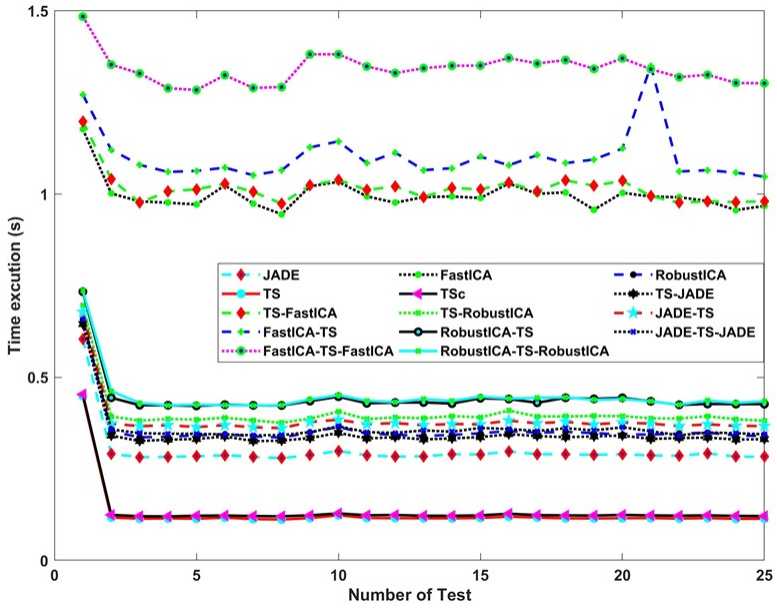

Figure 8.3: The time execution comparison.

amplitude and width of the Gaussian functions of the five PQRST waves). In this module, a number of kernels should be placed in the critical points of the ECG. Both automatic and manual beat fitter modules are tested, but the manual module is more robust. However, for the manual calculating the computational time is impossible since it ends when the user is done with choosing the kernels. On the other hand, in the automatic module based on the desired minimum error of the dynamic model the computational time varies. The average computational time in automatic EKF is 21.7 s.

8.4 Discussion

We compare different fECG extraction algorithms by assessing five well-defined criteria: the raw data, the motion noise, the white noise, the execution time, and the required memory. In pure data, we found that the F1 score widely ranges from 92.61% (TS-FastICA) to 54.34% (EKF). The results of TS algorithms are fairly consistent, and the same thing happened to ICA's. Algorithms with the same topology have relatively close F1 scores. TS algorithms

give better results than pure ICA algorithms, and when we combine them, we get a higher F1 score. With motion noise added, algorithms such as EKF and ICA have accuracy reduced by only 1% to 3%. However, for TS algorithms, F1-score was reduced by more than 11%. Overall, JADE-TS-JADE has the best performance and has the highest accuracy. However, RobustICA-TS shows the lowest accuracy reduction after adding motion noise. In other words, RobustICA-TS is more robust. According to results presented in Table 8.2, JADE-TS-JADE has the least F1 scores lower than 50% and EKF has the most F1 scores lower than 50% indicating the reliability and consistency of the methods. Although, the result of JADE-TS-JADE is the most reliable; the EKF algorithm only requires one channel for data acquisition and fECG extraction, while other methods need four channels of aECG. This indicates that with EKF, the physical device would be smaller and more unobtrusive.

Figure 8.2 illustrates the performance of algorithms in the presence of white noise with different amplitudes. In high SNR (low white noise), TS-FastICA has the best performance while in low SNR (high white noise), TS-JADE works better. Note that in very low SNR, data were completely corrupted, and the performance of different methods was found similar.

The next criterion is allocated memory for fECG extraction. Table 8.3 presents the required memory for these methods. The required memory for all methods was less than 1300 MB, except EKF. EKF needs much more memory for fECG extraction. Since for home-based monitoring, algorithms run on microprocessors, the required memory could be important. Figure 8.3 shows the computational time for these methods (excluding EKF). Execution time is vastly different. TS algorithms need the least time: 0.128 s, while that of FastICA -TS-FastICA is 1.5 s, which is the slowest running algorithm. We could see that 4 algorithms containing FastICA are very slow. The reason is that in some cases, the FastICA algorithm did not converge, depending on several initial values, while other algorithms are quite stable. If we remove those cases, the execution time of these algorithms will be approximately that of the same topology algorithms.

We noticed that the execution time of TS and TSc is the shortest. The execution time of algorithms containing FastICA and RobustICA (such as FastICA-TS and RobustICA-TS; TS-FastICA and TS-RobustICA, etc.) is nearly equal. Meanwhile, if we replace FastICA or RobustICA in those algorithms with JADE, it would take less time. In addition, we observed that JADE-TS runs slower than JADE-TS-JADE. The reason is that JADE-TS takes more time in the block fQRS detection and selection. The same thing happens with FastICA-TS and FastICA-TS-FastICA pairs. However, the advent of high-speed processors has made this factor less important.

Chapter 9

Conclusion and Prospective

9.1 Summary of contributions

This thesis provides a number of contributions to the field of non-invasive fetal electrocardiogram (NI-fECG) extraction and ECG analysis; (1) performed and presented a comprehensive comparison among different methods for NI-fECG extraction; (2) introduction of the Ensemble Kalman Filter as a Kamlan filtering technique for its application to NI-fECG extraction; (3) benchmark and evaluate the performance of the novel algorithm with existing technique (EKF); (4) developed a novel wearable fECG monitoring system consisting of an abdominal patch that communicates with a smart device; (5) development of our own clinical data.

This thesis focuses on the processing of the abdominal electrocardiogram (aECG) recorded to extract fECG signal. The proposed algorithm for fECG extraction offers many advantages over other fetal monitoring techniques, such as accuracy and robustness, enabling morphological analysis of the fECG and continuous monitoring of fetal heart rate (fHR).

9.2 Conclusion

9.2.1 fECG extraction Algorithms

An accurate fHR monitoring would provide valuable information that could help deliver better home-based fetal monitoring. In this thesis, we presented a comprehensive comparison among different methods for fECG extraction. Accuracy, feasibility, robustness and simplicity were utilized as criteria to compare, for those who are considering of selecting the most appropriate algorithm for their particular systems. For home-based fetal monitoring, the signal is most likely messed with motion artifacts; therefore, the performance of an algorithm in data with motion is preferred. In this case, JADE-TS-JADE showed the best performance in terms of aforementioned criteria. The EKF has the weakest performance, especially with noise added; however, it requires only one channel for fECG extraction, thus bringing compactness in manufacturing, and thus possibly being widely accepted by users. For future work, our team will focus on cloud-based analytics of fHR/fECG and maternal electrocardiogram (mECG) for promoting maternity care as well as novel algorithms to reliably extract fECG with full features of P waves, QRS complexes and T waves for early detection of congenital heart disease and critical events during pregnancy.

9.2.2 Home-based Fetal Electrocardiogram (ECG) Monitoring System

Currently, there is no such kind of highly-integrative system for home-based fetal and maternal monitoring. It was reported that pregnant women and their fetuses are more vulnerable to adverse outcomes and disease complications [102]. According to another research, the COVID-19 can accelerate pregnancy-related diseases [103]. Thus, in special scenarios such as the current COVID-19 pandemic, effective distanced care and monitoring are in need

more than ever. Our proposed system takes the burgeoning field of telemedicine and mobile health (m-Health) to the next level. Successful completion of this project provided a foundation to improve the infrastructure for providing remote monitoring to patients and care teams. To evaluate the efficiency and accuracy of the proposed method, we employed data to be obtained in the University of California, Irvine Medical Center under our the Proof of Product (POP) grant activity (see 4.2.2, and 5.3.2). The development of a home-based fECG monitoring system can be widely used due to 1) low cost, 2) compact and unobtrusive device, 3) high reliability, and 4) continuously monitor the fetal and maternal's heart rate. Figures 9.1a, 9.1b show the fetal ECG monitoring system in operation. The electrode patch attached to the maternal abdomen, which the app connects to the fetal patch through BLE protocols. The main interface of the app is shown in Figure 9.1c.

(a) (b) (c)

Figure 9.1: The fetal ECG monitoring system in operation. (a) Wearable fECG monitoring system attached to the maternal abdomen; (b) Wearable fECG monitoring system attached to the maternal abdomen; and (c) Android phone client main interface.

9.2.3 A Novel Algorithm for fECG Extraction

Current systems do not provide fECG with full features of PQRST waves which show the functional conditions of the heart. Thus, Continuous fECG monitoring would provide not

only additional information for Congenital heart disease (CHD) detection but also the progression toward abnormal development. Further, continuous fECG monitoring in the home setting would be invaluable for prognosis as well as studies for therapeutic potentials. We have implemented different extraction combined algorithms and validated them using the modified online data with Gaussian and motion noise added, mimicking practical scenarios (See Chapter 8). There is no approach available to extract fetal characteristic waves [13]. In the clinics, we performed one-channel ECG acquisition and we applied a proposed algorithm, the EnKF. the EnKF is a Sequential Monte Carlo (SMC) method, and it shows a better performance, especially in systems with strong nonlinearity than the popular Extended Kalman filter (EKF) that applies analytic linearization. We used the EnKF algorithm to extract fECG which exhibits robust and efficient performance. We have found the EnKF would yield superior performance. Finally, after deploying sequential EnKF to extract fECG with characteristic features, as results in 6.4 the segments and intervals would be measured.

We first tested and compared the performance of EKF and EnKF with noise-added aECG signals. We further validated the algorithms on 10-20 pregnant women during the 2nd or 3rd trimester in different types of activity such as walking or jogging at different speeds. We carried this out in the UCI Medical Center (see 4.2.2). As was shown in this thesis, the EnKF method relies on accurate and precise fQRS and mQRS detection.

9.2.4 Novel Algorithm for ECG denoising

The ECG has always been a popular measurement scheme to assess and diagnose cardiovascular diseases (CVDs) [104]. ECG will provide vital information about fHR, and the existence of abnormalities or distress in the heart. The precise ECG depicts PQRST features in the signal that helps evaluate the functional status of the heart. The high noise level in daily life renders long-entrenched challenges to monitoring ECG signals. In this

thesis, we proposed a novel algorithm. the EnKF, to denoise ECG signal. This algorithm is to develop a robust scheme to provide home-based HR monitoring from a compact device with the presence of high noise. To evaluate the novel algorithm, we first test it with online databanks (see 4.2.3). We further validated it with modified signals with motional artifacts added (see 4.2.4). The results of this thesis approve the applicability of the EnKF, for the filtering of noisy ECG signals.

9.3 Future works

A number of general items identified for future works are summarised below.

- Conduct more experiments on the pregnant subjects, including subjects with twins and multi-fetal prenatal, to validate the system and the fECG extraction algorithms, could be conducted.
- Improve the entire fetal monitoring system with more miniaturized patches, optimized Android and iOS apps, real-time and pseudo-real time analytics with cloud computing.
- Evaluate the proposed denoising algorithm, EnKF, in the home setting device.
- Assess the fECG patch and the EnKF algorithm in out-of-clinic settings.
- Correlate with other physiological signals to link the mother's activity with fetal development [14, 105].
- Find the optimal electrode placement for recording high-quality fetal ECG signal for further processing.

Bibliography

[1] JeroenGustaaf Stinstra. Reliability of the fetal magnetocardiogram. 2003.

[2] Radek Martinek, Jan Nedoma, Marcel Fajkus, Radana Kahankova, Jaromir Konecny, Petr Janku, Stanislav Kepak, Petr Bilik, and Homer Nazeran. A phonocardiographic-based fiber-optic sensor and adaptive filtering system for noninvasive continuous fetal heart rate monitoring. *Sensors*, 17(4):890, 2017.

[3] Paul Porter, Fleur Muirhead, Joanna Brisbane, Brooke Schneider, Jennifer Choveaux, Natasha Bear, Jennie Carson, Kym Jones, Desiree Silva, and Cliff Neppe. Accuracy, clinical utility, and usability of a wireless self-guided fetal heart rate monitor. *Obstetrics and Gynecology*, 137(4):673, 2021.

[4] Radana Kahankova, Radek Martinek, Rene Jaros, Khosrow Behbehani, Adam Matonia, Michal Jezewski, and Joachim A Behar. A review of signal processing techniques for non-invasive fetal electrocardiography. *IEEE reviews in biomedical engineering*, 13:51–73, 2019.

[5] Rene Jaros, Radek Martinek, and Radana Kahankova. Non-adaptive methods for fetal ecg signal processing: a review and appraisal. *Sensors*, 18(11):3648, 2018.

[6] `https://www.usa.philips.com/healthcare/product/HC866488/avalon-beltless-fetal-monitoring-solution`.

[7] Melanie P Heron. Deaths: leading causes for 2016. 2018.

[8] Elizabeth Wilkins, L Wilson, Kremlin Wickramasinghe, Prachi Bhatnagar, Jose Leal, Ramon Luengo-Fernandez, R Burns, Mike Rayner, and Nick Townsend. European cardiovascular disease statistics 2017. 2017.

[9] Elizabeth CW Gregory. *Trends in fetal and perinatal mortality in the United States, 2006-2012*. Number 169. US Department of Health and Human Services, Centers for Disease Control and ..., 2014.

[10] Marian F MacDorman and Sharon Kirmeyer. Fetal and perinatal mortality: United states, 2005. 2009.

[11] Rene Jaros, Radana Kahankova, Radek Martinek, Jan Nedoma, Marcel Fajkus, and Zdenek Slanina. Fetal phonocardiography signal processing from abdominal records

by non-adaptive methods. In *Photonics Applications in Astronomy, Communications, Industry, and High-Energy Physics Experiments 2018*, volume 10808, page 108083E. International Society for Optics and Photonics, 2018.

[12] Laura D Zambrano, Sascha Ellington, Penelope Strid, Romeo R Galang, Titilope Oduyebo, Van T Tong, Kate R Woodworth, John F Nahabedian III, Eduardo Azziz-Baumgartner, Suzanne M Gilboa, et al. Update: characteristics of symptomatic women of reproductive age with laboratory-confirmed sars-cov-2 infection by pregnancy status—united states, january 22–october 3, 2020. *Morbidity and Mortality Weekly Report*, 69(44):1641, 2020.

[13] Sadaf Sarafan, Tai Le, Amir Mohammad Naderi, Quoc-Dinh Nguyen, Brandon Tiang-Yu Kuo, Tadesse Ghirmai, Huy-Dung Han, Michael PH Lau, and Hung Cao. Investigation of methods to extract fetal electrocardiogram from the mother's abdominal signal in practical scenarios. *Technologies*, 8(2):33, 2020.

[14] Sadaf Sarafan, Tai Le, Floranne Ellington, Zhijie Zhang, Michael PH Lau, Tadesse Ghirmai, Afshan Hameed, and Hung Cao. Development of a home-based fetal electrocardiogram (ecg) monitoring system. pages 7116–7119, 2021.

[15] Sadaf Sarafan, Tai N Le, Michael PH Lau, Afshan Hameed, Tadesse Ghirmai, and Hung Cao. Fetal electrocardiogram extraction from the mother's abdominal signal using the ensemble kalman filter. *bioRxiv*, 2021.

[16] Sadaf Sarafan, Hoang Vuong, Daniel Jilani, Michael PH Lau, Tadesse Ghirmai, and Hung Cao. A novel ecg denoising scheme using the ensemble kalman filter. In *2021 44rd Annual International Conference of the IEEE Engineering in Medicine & Biology Society (EMBC)*, pages 7116–7119. IEEE, 2022.

[17] Peter L Houtekamer and Fuqing Zhang. Review of the ensemble kalman filter for atmospheric data assimilation. *Monthly Weather Review*, 144(12):4489–4532, 2016.

[18] Peter W Macfarlane, Adriaan Van Oosterom, Olle Pahlm, Paul Kligfield, Michiel Janse, and John Camm. *Comprehensive electrocardiology*. Springer Science & Business Media, 2010.

[19] Pentti M Rautaharju. Eyewitness to history: Landmarks in the development of computerized electrocardiography. *Journal of Electrocardiology*, 49(1):1–6, 2016.

[20] Reza Sameni. *Extraction of fetal cardiac signals from an array of maternal abdominal recordings*. PhD thesis, Institut National Polytechnique de Grenoble-INPG; Sharif University of ..., 2008.

[21] Andreea A Creanga and William M Callaghan. Recent increases in the us maternal mortality rate: disentangling trends from measurement issues. *Obstetrics & Gynecology*, 129(1):206–207, 2017.

[22] Saeed Dastgiri, DH Stone, C Le-Ha, and WHl Gilmour. Prevalence and secular trend of congenital anomalies in glasgow, uk. *Archives of disease in childhood*, 86(4):257–263, 2002.

[23] Fay Menacker and Joyce A Martin. Expanded health data from the new birth certificate, 2005. 2008.

[24] Eva Pajkrt, Boaz Weisz, Helen V Firth, and Lyn S Chitty. Fetal cardiac anomalies and genetic syndromes. *Prenatal Diagnosis: Published in Affiliation With the International Society for Prenatal Diagnosis*, 24(13):1104–1115, 2004.

[25] Janusz Jezewski, Dawid Roj, Janusz Wrobel, and Krzysztof Horoba. A novel technique for fetal heart rate estimation from doppler ultrasound signal. *Biomedical engineering online*, 10(1):1–17, 2011.

[26] J-F Cardoso. Blind signal separation: statistical principles. *Proceedings of the IEEE*, 86(10):2009–2025, 1998.

[27] Jr Charles A Hunter, Robert J Braunlin, Kenneth G Lansford, and Suzanne B Knoebel. Method for obtaining a fetal electrocardiogram, February 4 1964. US Patent 3,120,227.

[28] Peter Varady, Ludwig Wildt, Zoltan Benyo, and Achim Hein. An advanced method in fetal phonocardiography. *Computer Methods and programs in Biomedicine*, 71(3):283–296, 2003.

[29] Reza Sameni and Gari D Clifford. A review of fetal ecg signal processing; issues and promising directions. *The open pacing, electrophysiology & therapy journal*, 3:4, 2010.

[30] Agnese Sbrollini, Annachiara Strazza, Manila Caragiuli, Claudia Mozzoni, Selene Tomassini, Angela Agostinelli, Micaela Morettini, Sandro Fioretti, Francesco Di Nardo, and Laura Burattini. Fetal phonocardiogram denoising by wavelet transformation: robustness to noise. In *2017 Computing in Cardiology (CinC)*, pages 1–4. IEEE, 2017.

[31] Henk W Jongsma, Adriaan van Oosterom, Henry G Murray, and Herman P van Geijn. Introduction to fetal electrocardiography. 1986.

[32] Maria Peters, John Crowe, Jean-Francois Piéri, Hendrik Quartero, Barrie Hayes-Gill, David James, Jeroen Stinstra, and Simon Shakespeare. Monitoring the fetal heart non-invasively: a review of methods. 2001.

[33] DJ Jagannath and A Immanuel Selvakumar. Issues and research on foetal electrocardiogram signal elicitation. *Biomedical signal processing and control*, 10:224–244, 2014.

[34] Reza Sameni, Mohammad B Shamsollahi, Christian Jutten, and Gari D Clifford. A nonlinear bayesian filtering framework for ecg denoising. *IEEE Transactions on Biomedical Engineering*, 54(12):2172–2185, 2007.

[35] Joachim Behar, Fernando Andreotti, Sebastian Zaunseder, Qiao Li, Julien Oster, and Gari D Clifford. An ecg simulator for generating maternal-foetal activity mixtures on abdominal ecg recordings. *Physiological measurement*, 35(8):1537, 2014.

[36] Radek Martinek, Michal Kelnar, Petr Koudelka, Jan Vanus, Petr Bilik, Petr Janku, Homer Nazeran, and Jan Zidek. A novel labview-based multi-channel non-invasive abdominal maternal-fetal electrocardiogram signal generator. *Physiological measurement*, 37(2):238, 2016.

[37] Reza Sameni, Christian Jutten, and Mohammad B Shamsollahi. Multichannel electrocardiogram decomposition using periodic component analysis. *IEEE transactions on biomedical engineering*, 55(8):1935–1940, 2008.

[38] Muhammad Asfarul Hasan, MBI Reaz, MI Ibrahimy, MS Hussain, and J Uddin. Detection and processing techniques of fecg signal for fetal monitoring. *Biological procedures online*, 11(1):263–295, 2009.

[39] Wayne R Cohen and Barrie Hayes-Gill. Influence of maternal body mass index on accuracy and reliability of external fetal monitoring techniques. *Acta obstetricia et gynecologica Scandinavica*, 93(6):590–595, 2014.

[40] Carol Rados. Fda cautions against ultrasound "keepsake" images. *FDA Consumer Magazine. www. fda. gov/fdac/features/2004/104_images. html. Accessed*, 11, 2005.

[41] J Adam. The future of fetal monitoring. *Reviews in obstetrics and gynecology*, 5(3-4):e132, 2012.

[42] Radek Martinek, Radana Kahankova, Janusz Jezewski, Rene Jaros, Jitka Mohylova, Marcel Fajkus, Jan Nedoma, Petr Janku, and Homer Nazeran. Comparative effectiveness of ica and pca in extraction of fetal ecg from abdominal signals: Toward non-invasive fetal monitoring. *Frontiers in physiology*, 9:648, 2018.

[43] Luay Yassin Taha and Esam Abdel-Raheem. Extraction of fetal electrocardiogram signals using blind source extraction based parallel linear predictor filter. In *2018 IEEE International Symposium on Signal Processing and Information Technology (ISSPIT)*, pages 208–211. IEEE, 2018.

[44] Luay Yassin Taha and Esam Abdel-Raheem. Efficient blind source extraction of noisy mixture utilising a class of parallel linear predictor filters. *IET Signal Processing*, 12(8):1009–1016, 2018.

[45] Aapo Hyvärinen and Erkki Oja. Independent component analysis: algorithms and applications. *Neural networks*, 13(4-5):411–430, 2000.

[46] Tai Le, Joseph Fortunato, Nicholas Maritato, Yeeun Cho, Quoc-Dinh Nguyen, Tadesse Ghirmai, Michael PH Lau, Huy-Dung Han, Cuong Kieu Nguyen, Vu Cong Nguyen, et al. Home-based mobile fetal/maternal electrocardiogram acquisition and extraction with cloud assistance. In *2019 IEEE MTT-S International Microwave Biomedical Conference (IMBioC)*, volume 1, pages 1–4. IEEE, 2019.

[47] Utako Yamamoto, Yuka Nakamura, Hisatake Yokouchi, and Tomoyuki Hiroyasu. Improving the accuracy of the method for removing motion artifacts from fnirs data using ica and an accelerometer. In *2014 World Automation Congress (WAC)*, pages 131–136. IEEE, 2014.

[48] Qiong Yu, Huawen Yan, Lin Song, Wenya Guo, Hongxing Liu, Junfeng Si, and Ying Zhao. Automatic identifying of maternal ecg source when applying ica in fetal ecg extraction. *Biocybernetics and Biomedical Engineering*, 38(3):448–455, 2018.

[49] Joachim Behar, Julien Oster, and Gari D Clifford. Combining and benchmarking methods of foetal ecg extraction without maternal or scalp electrode data. *Physiological measurement*, 35(8):1569, 2014.

[50] Kwang Jin Lee and Boreom Lee. Sequential total variation denoising for the extraction of fetal ecg from single-channel maternal abdominal ecg. *Sensors*, 16(7):1020, 2016.

[51] He Liu, Deyun Chen, and Guanghao Sun. Detection of fetal ecg r wave from single-lead abdominal ecg using a combination of rr time-series smoothing and template-matching approach. *IEEE Access*, 7:66633–66643, 2019.

[52] Mihaela Ungureanu, Johannes WM Bergmans, Swan Guid Oei, and Rodica Strungaru. Fetal ecg extraction during labor using an adaptive maternal beat subtraction technique. 2007.

[53] M Varanini, G Tartarisco, L Billeci, A Macerata, G Pioggia, and R Balocchi. An efficient unsupervised fetal qrs complex detection from abdominal maternal ecg. *Physiological measurement*, 35(8):1607, 2014.

[54] Sebastian Zaunseder, Fernando Andreotti, Marcos Cruz, Holger Stepan, Claudia Schmieder, Hagen Malberg, Alexander Jank, and Niels Wessel. Fetal qrs detection by means of kalman filtering and using the event synchronous canceller. In *Proceedings of the 7th International Workshop on Biosignal Interpretation, Como, Italy*, pages 2–4, 2012.

[55] Adam Matonia, Janusz Jezewski, Krzysztof Horoba, Adam Gacek, and P Labaj. The maternal ecg suppression algorithm for efficient extraction of the fetal ecg from abdominal signal. In *2006 International Conference of the IEEE Engineering in Medicine and Biology Society*, pages 3106–3109. IEEE, 2006.

[56] Eleni Fotiadou, Judith OEH Van Laar, S Guid Oei, and Rik Vullings. Enhancement of low-quality fetal electrocardiogram based on time-sequenced adaptive filtering. *Medical & biological engineering & computing*, 56(12):2313–2323, 2018.

[57] Abdullah Mohammed Kaleem and Rajendra D Kokate. An efficient adaptive filter for fetal ecg extraction using neural network. *Journal of Intelligent Systems*, 28(4):589–600, 2019.

[58] Radek Martinek, Radana Kahankova, Homer Nazeran, Jaromir Konecny, Janusz Jezewski, Petr Janku, Petr Bilik, Jan Zidek, Jan Nedoma, and Marcel Fajkus. Non-invasive fetal monitoring: A maternal surface ecg electrode placement-based novel approach for optimization of adaptive filter control parameters using the lms and rls algorithms. *Sensors*, 17(5):1154, 2017.

[59] Shuicai Wu, Yanni Shen, Zhuhuang Zhou, Lan Lin, Yanjun Zeng, and Xiaofeng Gao. Research of fetal ecg extraction using wavelet analysis and adaptive filtering. *Computers in biology and medicine*, 43(10):1622–1627, 2013.

[60] Fernando Andreotti, Maik Riedl, Tilo Himmelsbach, Daniel Wedekind, Sebastian Zaunseder, Niels Wessel, and Hagen Malberg. Maternal signal estimation by kalman filtering and template adaptation for fetal heart rate extraction. In *Computing in Cardiology 2013*, pages 193–196. IEEE, 2013.

[61] M Suganthy and S Manjula. Enhancement of snr in fetal ecg signal extraction using combined swt and wlsr in parallel ekf. *Cluster Computing*, 22(2):3875–3881, 2019.

[62] Rik Vullings, Bert De Vries, and Jan WM Bergmans. An adaptive kalman filter for ecg signal enhancement. *IEEE transactions on biomedical engineering*, 58(4):1094–1103, 2010.

[63] S Hema Jothi and K Helen Prabha. Fetal electrocardiogram extraction using adaptive neuro-fuzzy inference systems and undecimated wavelet transform. *IETE Journal of Research*, 58(6):469–475, 2012.

[64] Radek Martinek, Radana Kahankova, Jan Nedoma, Marcel Fajkus, and Kristyna Cholevova. Fetal ecg preprocessing using wavelet transform. In *Proceedings of the 10th International Conference on Computer Modeling and Simulation*, pages 39–43, 2018.

[65] Manuja Sharma, Peter Ritchie, Tadesse Ghirmai, Hung Cao, and Michael PH Lau. Unobtrusive acquisition and extraction of fetal and maternal ecg in the home setting. In *2017 IEEE SENSORS*, pages 1–3. IEEE, 2017.

[66] Jean-François Cardoso and Antoine Souloumiac. Blind beamforming for non-gaussian signals. In *IEE proceedings F (radar and signal processing)*, volume 140, pages 362–370. IET, 1993.

[67] Jean-François Cardoso. High-order contrasts for independent component analysis. *Neural computation*, 11(1):157–192, 1999.

[68] Vicente Zarzoso and Pierre Comon. Robust independent component analysis by iterative maximization of the kurtosis contrast with algebraic optimal step size. *IEEE Transactions on neural networks*, 21(2):248–261, 2009.

[69] Suzanna MM Martens, Chiara Rabotti, Massimo Mischi, and Rob J Sluijter. A robust fetal ecg detection method for abdominal recordings. *Physiological measurement*, 28(4):373, 2007.

[70] Sergio Cerutti, Giuseppe Baselli, Silvia Civardi, Enrico Ferrazzi, Anna Maria Marconi, Massimo Pagani, and Giorgio Pardi. Variability analysis of fetal heart rate signals as obtained from abdominal electrocardiographic recordings. 1986.

[71] Joachim Behar, Julien Oster, and Gari D Clifford. *Non-invasive FECG extraction from a set of abdominal sensors*. IEEE, 2013.

[72] Jiapu Pan and Willis J Tompkins. A real-time qrs detection algorithm. *IEEE transactions on biomedical engineering*, (3):230–236, 1985.

[73] A Karimi Rahmati, SK Setarehdan, and BN Araabi. A pca/ica based fetal ecg extraction from mother abdominal recordings by means of a novel data-driven approach to fetal ecg quality assessment. *Journal of biomedical physics & engineering*, 7(1):37, 2017.

[74] Ikaro Silva, Joachim Behar, Reza Sameni, Tingting Zhu, Julien Oster, Gari D Clifford, and George B Moody. Noninvasive fetal ecg: the physionet/computing in cardiology challenge 2013. In *Computing in Cardiology 2013*, pages 149–152. IEEE, 2013.

[75] George B Moody and Roger G Mark. The mit-bih arrhythmia database on cd-rom and software for use with it. In *[1990] Proceedings Computers in Cardiology*, pages 185–188. IEEE, 1990.

[76] Hung Cao, Fei Yu, Yu Zhao, Xiaoxiao Zhang, Joyce Tai, Juhyun Lee, Ali Darehzereshki, Malcolm Bersohn, Ching-Ling Lien, Neil C Chi, et al. Wearable multi-channel microelectrode membranes for elucidating electrophysiological phenotypes of injured myocardium. *Integrative Biology*, 6(8):789–795, 2014.

[77] EM Graatsma, BC Jacod, LAJ Van Egmond, EJH Mulder, and GHA Visser. Fetal electrocardiography: feasibility of long-term fetal heart rate recordings. *BJOG: An International Journal of Obstetrics & Gynaecology*, 116(2):334–338, 2009.

[78] Rudolph Emil Kalman. A new approach to linear filtering and prediction problems. 1960.

[79] Andrew H Jazwinski. *Stochastic processes and filtering theory*. Courier Corporation, 2007.

[80] Geir Evensen. Sequential data assimilation with a nonlinear quasi-geostrophic model using monte carlo methods to forecast error statistics. *Journal of Geophysical Research: Oceans*, 99(C5):10143–10162, 1994.

[81] A UmaMageswari, J Joseph Ignatious, and R Vinodha. A comparitive study of kalman filter, extended kalman filter and unscented kalman filter for harmonic analysis of the non-stationary signals. *International Journal of Scientific & Engineering Research*, 3(7):1–9, 2012.

[82] Johannes Keller, Harrie-Jan Hendricks Franssen, and Gabriele Marquart. Comparing seven variants of the ensemble kalman filter: How many synthetic experiments are needed? *Water Resources Research*, 54(9):6299–6318, 2018.

[83] Brian DO Anderson and John B Moore. *Optimal filtering*. Courier Corporation, 2012.

[84] Matthias Katzfuss, Jonathan R Stroud, and Christopher K Wikle. Understanding the ensemble kalman filter. *The American Statistician*, 70(4):350–357, 2016.

[85] Patrick E McSharry, Gari D Clifford, Lionel Tarassenko, and Leonard A Smith. A dynamical model for generating synthetic electrocardiogram signals. *IEEE transactions on biomedical engineering*, 50(3):289–294, 2003.

[86] Yuxin Zhao, Carsten Fritsche, Feng Yin, Fredrik Gunnarsson, and Fredrik Gustafsson. Sequential monte carlo methods and theoretical bounds for proximity report based indoor positioning. *IEEE Transactions on Vehicular Technology*, 67(6):5372–5386, 2018.

[87] Patrizia Ciarlini and Piero Barone. A recursive algorithm to compute the baseline drift in recorded biological signals. *Computers and biomedical research*, 21(3):221–226, 1988.

[88] CR Meyer and HN Keiser. Electrocardiogram baseline noise estimation and removal using cubic splines and state-space computation techniques. *Computers and Biomedical Research*, 10(5):459–470, 1977.

[89] Seyfullah Halit Oguz and Muka Hakan Asyali. A morphology based algorithm for baseline wander elimination in ecg records. In *Proceedings of the 1992 International Biomedical Engineering Days*, pages 157–160. IEEE, 1992.

[90] Jan A Van Alste, W Van Eck, and OE Herrmann. Ecg baseline wander reduction using linear phase filters. *Computers and Biomedical Research*, 19(5):417–427, 1986.

[91] Donald P Golden Jr, GW Hoffler, Roger A Wolthuis, and Robert L Johnson. Vectan ii: A computer program for the spatial analysis of the vectorcardiogram. *Journal of electrocardiology*, 8(3):217–225, 1975.

[92] Jake R Gradwohl, Erik W Pottala, Martha R Horton, and James J Bailey. Comparison of two methods for removing baseline wander in the ecg. In *Proceedings. Computers in Cardiology 1988*, pages 493–496. IEEE, 1988.

[93] T Kohl, A Müller, K Tchatcheva, S Achenbach, and U Gembruch. Fetal transesophageal echocardiography: clinical introduction as a monitoring tool during cardiac intervention in a human fetus. *Ultrasound in Obstetrics and Gynecology: The Official Journal of the International Society of Ultrasound in Obstetrics and Gynecology*, 26(7):780–785, 2005.

[94] Jack Rychik, Nancy Ayres, Bettina Cuneo, Nina Gotteiner, Lisa Hornberger, Philip J Spevak, and Mary Van Der Veld. American society of echocardiography guidelines and standards for performance of the fetal echocardiogram. *Journal of the American Society of Echocardiography*, 17(7):803–810, 2004.

[95] Nicole Corsten-Janssen, Katelijne Bouman, Janouk CD Diphoorn, Arjen J Scheper, Rianne Kinds, Julia El Mecky, Hanna Breet, Joke BGM Verheij, Ron Suijkerbuijk, Leonie K Duin, et al. A prospective study on rapid exome sequencing as a diagnostic test for multiple congenital anomalies on fetal ultrasound. *Prenatal diagnosis*, 40(10):1300–1309, 2020.

[96] Mohammed AlMahamdy and H Bryan Riley. Performance study of different denoising methods for ecg signals. *Procedia Computer Science*, 37:325–332, 2014.

[97] Reza Sameni, MB Shamsollahi, and Christian Jutten. Filtering electrocardiogram signals using the extended kalman filter. In *2005 IEEE Engineering in Medicine and Biology 27th Annual Conference*, pages 5639–5642. IEEE, 2006.

[98] Li Zebin, Lu Wei, Gao Lifu, and Zhang Jinsi. Research on ecg denoising method based on empirical mode decomposition and wavelet transform. In *2020 IEEE 5th International Conference on Signal and Image Processing (ICSIP)*, pages 675–679. IEEE, 2020.

[99] Kang-Ming Chang. Arrhythmia ecg noise reduction by ensemble empirical mode decomposition. *Sensors*, 10(6):6063–6080, 2010.

[100] S Sachin Kumar, Neethu Mohan, P Prabaharan, and KP Soman. Total variation denoising based approach for r-peak detection in ecg signals. *Procedia Computer Science*, 93:697–705, 2016.

[101] Nasser Mourad. Ecg denoising algorithm based on group sparsity and singular spectrum analysis. *Biomedical Signal Processing and Control*, 50:62–71, 2019.

[102] John N Hansen, Jason Hine, and Tania D Strout. Covid-19 and preeclampsia with severe features at 34-weeks gestation. *The American journal of emergency medicine*, 39:252–e3, 2021.

[103] Hillary Hosier, Shelli F Farhadian, Raffaella A Morotti, Uma Deshmukh, Alice Lu-Culligan, Katherine H Campbell, Yuki Yasumoto, Chantal BF Vogels, Arnau Casanovas-Massana, Pavithra Vijayakumar, et al. Sars–cov-2 infection of the placenta. *The Journal of clinical investigation*, 130(9):4947–4953, 2020.

[104] Mohamed Adel Serhani, Hadeel T El Kassabi, Heba Ismail, and Alramzana Nujum Navaz. Ecg monitoring systems: Review, architecture, processes, and key challenges. *Sensors*, 20(6):1796, 2020.

[105] Khuong Vo, Emad Kasaeyan Naeini, Amir Naderi, Daniel Jilani, Amir M Rahmani, Nikil Dutt, and Hung Cao. P2e-wgan: Ecg waveform synthesis from ppg with conditional wasserstein generative adversarial networks. In *Proceedings of the 36th Annual ACM Symposium on Applied Computing*, pages 1030–1036, 2021.